Spring 2017

The bovine serum albumin protein corona on nanoparticles: investigating the effects of changing pH, substrates, and ions

Brittany Estelle Givens
University of Iowa

THE BOVINE SERUM ALBUMIN PROTEIN CORONA ON NANOPARTICLES: INVESTIGATING THE EFFECTS OF CHANGING pH, SUBSTRATES, AND IONS

by

Brittany Estelle Givens

A thesis submitted in partial fulfillment
of the requirements for the Master of Science
degree in Chemical and Biochemical Engineering in the
Graduate College of
The University of Iowa

May 2017

Thesis Supervisors: Adjunct Professor Dr. Vicki H. Grassian
Associate Professor Dr. Jennifer Fiegel

Graduate College

The University of Iowa

Iowa City, Iowa

CERTIFICATE OF APPROVAL

_____

MASTER'S THESIS

_____

This is to certify that the Master's thesis of

Brittany Estelle Givens

has been approved by the Examining Committee for
the thesis requirement for the Master of Science degree
in Chemical and Biochemical Engineering at the May 2017 graduation.

Thesis Committee: _____
Vicki H. Grassian, Thesis Supervisor

_____
Jennifer Fiegel, Thesis Supervisor

_____
Aliasger K. Salem

To Mom and Dad

"We would accomplish many more things if we did not think of them as impossible"

Vince Lombardi, Jr.

Acknowledgements

I would like to thank my advisors, Dr. Vicki H. Grassian and Dr. Jennifer Fiegel, for their support and guidance throughout this project. The knowledge that I gained from working with them is invaluable and I hope to continue practicing what I learned during my time with them. I would also like to thank my thesis committee, Drs. Julie Jessop, Sarah Larsen, and Aliasger Salem for their guidance with this project. I would also like to thank my mentors, Drs. Charles Stanier, Tonya Peeples, Colleen Mitchell, Phil Kutzco, and Aliasger Salem for their support and guidance through graduate school with my both research and extracurricular activities.

I also thank all of my labmates in both the Grassian and Fiegel research groups. From the Grassian group I thank all of the post-doctoral researchers and senior graduate students for answering all of my questions, training me in the laboratory, and supporting me in ways that allowed me to succeed. Thanks to: Drs. Imali Mudunkotuwa, Armando Estillore, Richard Cochran, Olga Laskina, Aruni Gandanka, Mingjin Tang, and Jonathan Trueblood, Joshua Grandquist, Hayder Alawan, Alaa Al Minshid, Yuan Fang, Zhenzhu Xu. From the Fiegel lab I thank all the senior laboratory members that welcomed me and guided me through my research: Drs. Mai Tu and Daniel Schenck, and Benjamin King, Bharath Gowdampally, and Sachin Gharse. I also thank my peers, those who joined the Grassian lab alongside me or the Department of Chemical Engineering during the same year and provided much needed support these past two years: Ellen Coddens, Sanjaya Jayalath, Deokhyeon Kwon, Kaitlynn McElvain, Jiajie Qian, and Alan Rassoolkhani. I would also like to thank the undergraduate researchers without whom I would not have been as successful: Nina Diklich, Sarah Goettler, and Elizabeth Wilson. Finally, I would like to thank all of my other friends in the Iowa City area for making me feel welcome and at home during my studies.

I would also like to thank Dr. Joun (Sylvia) Lee for her help with my project during her time with the Central Microscopy Research Facilities at UIowa. I would also like to thank the support staff, including Katie Schnedler and Jacquie Albrecht from Chemical Engineering for their support and dedication to helping graduate students succeed.

An additional thank you to my family and closest friends including my mother and father, Sharon and Anthony Givens, for always believing in me from the beginning. Without the continued support of my friends and family, I would not have been able to succeed in this program.

Abstract

Nanoparticles are currently used in a wide range of applications including industrially processes, consumer products, and as drug delivery vehicles. The potential toxicity of these nanoparticles in living organisms is concerning due to their ever-expanding applications and accumulation in the environment. The effects of properties of the human body on the potential harmful nature of these nanoparticles must be understood in order to ensure safety in workplaces and at-home products.

In this thesis, the interactions between nanoparticles and the most abundant blood protein, serum albumin, were investigated. The effects of changing the aqueous environment was investigated over a range of different pH values and with different ionic salts dissolved in water. The effects of changing the nanoparticle substrate were investigated to determine if different nanoparticles affect proteins differently. Finally, the effects of changing the concentration of nanoparticles and the presence of protein were investigated in a model lung cell line *in vitro*.

The studies over different pH values revealed that serum albumin was able to adsorb to the silica nanoparticle surface, and retained its secondary structure both as a function of pH and adsorption in a 2-hour time frame. However, adsorption was greater on the titanium dioxide nanoparticle surface and the protein lost secondary structure at acidic pH (pH 2.0). Studies with different ionic salts revealed a possible correlation between BSA adsorption and nanoparticle aggregation in that the attractive interactions between nanoparticles were least when the least amount of protein was adsorbed to the nanoparticle surface. *In vitro* studies with A549 human adenocarcinoma lung cells were inconclusive in determining the potential toxicity of these nanoparticles, but preliminary results suggested that the addition of protein to the system decreased toxicity compared with nanoparticles alone. This research aims to inform the field of

nanotechnology via investigating the safety and efficacy of nanoparticles before they reach the consumer.

Public abstract

The field of nanotechnology is rapidly growing and utilizes tiny particles for unique functions. The scientific advances in the field have led to an increase in nanoparticles used in common household products including: sunscreen, paints, and long-acting prescription drugs. However, harmful effects these nanoparticles may have on human health are widely unknown. The goal of this research is to investigate the properties of nanoparticles in the presence of the most-abundant blood protein to improve the understanding of nano-bio interactions. Studies were completed using a variety of aqueous solutions and comparing properties such as nanoparticle aggregation, protein adsorption to the nanoparticle surfaces, and the protein structure to determine whether these nanoparticles are harmful to biological components.

Silicon dioxide (silica) nanoparticles were chosen because they are used in all of the aforementioned products. The protein bovine serum albumin (BSA) was added to silica systems to investigate changes in the properties of the nanoparticles. Additionally, a model lung cell was used to determine the responses of the smallest living component to the human body. The results from this study suggest that silica nanoparticles are not harmful to human cells in low doses for short exposure times.

Table of contents

List of tables

List of figures

Chapter 1 Introduction

1.1 Properties and applications of nanoparticles

Nanotechnology offers many opportunities for improving materials and industries due to the unique properties at the nanoparticle surface. Nanoparticles are defined as particles with at least one dimension on the scale of 1 – 100 nm [1]. Due to their small size, nanoparticles behave differently than their bulk counterparts [2], and even particles in the micrometer size range [3]. These particles have a high surface area to volume ratio, resulting in a large amount of surface free energy [1, 4]. The surface properties of nanoparticles results in a wide range of applications, which are constantly growing and broadening [5, 6]. These applications can further be tailored by changing particle size and shape, as well as functionalizing nanoparticle surfaces [7-10].

Nanoparticles may come from natural sources, including volcanic eruptions, forest fires, dust storms, and oceans [3, 11]. They may also come from man-made sources, such as diesel exhaust, drug delivery vehicles, cigarette smoke, or be made intentionally for various industries [3, 5, 11]. The disposal of these nanoparticles is not well controlled, and they may remain in the environment for long periods of time [5, 12-14]. As such, there is great potential for nanoparticles to interact with living organisms [12, 13, 15, 16], and their potential effects on human health are of increasing interest [2, 17].

Among the major disadvantages to increased nanoparticle use is their accumulation in solid and aqueous environments [5, 16]. In aqueous environments, metal and metal oxide nanoparticles may undergo dissolution and leach metal ions [4, 18-21]. They may also undergo aggregation, increasing the overall particle diameter, and decreasing nanoparticle stability in solution [4, 20-23]. Intact nanoparticles have a complex surface morphology arising from different crystalline

structures, and as such, these particles have highly reactive surface sites [4]. This variety of crystal planes also increases the available surface energy at the surface of these nanoparticles [1, 4]. A number of more recent studies have also noted an increase in surface enthalpy of certain metal oxide nanoparticles, in addition to the increased surface energy [24, 25]. The increase in surface enthalpy of these particles, increases the affinity for other molecules towards the particle surface [24, 25].

Engineered, or man-made, nanoparticles may be intentionally designed for human use. These materials include titanium dioxide in food additives [26], iron oxides for magnetic resonance imaging (MRI) [27], nano-silver for antimicrobial and biosensing applications, nano-gold for biosensing and drug delivery [27], and silicon dioxide (silica) for sustained-release drug delivery vehicles or food additives [28-30]. Nanoparticle-based drug delivery is an increasingly popular area of research for therapeutic applications, targeted gene delivery, and sustained release (long-term) drug delivery systems [27, 31, 32].

Inhaled, or nasal, delivery is advantageous for diseased lungs because drugs do not have to pass through the entire circulatory system before reaching the target organ [33], and they bypass the harsh environments of the stomach and intestines from oral delivery [34]. Furthermore, one of the most widely used cell lines for nanotoxicity, A549 cells, originate from diseased lungs [35]. However, there are still challenges that face pulmonary drug delivery which include: effectively reaching on the target site [36], particle processing after delivery [37], and uptake efficiency [38]. Additionally, A549 cells do not provide a good model for all lung diseases, or healthy lungs [39, 40]. However, they are a good first step towards understanding what may occur in complex systems [41].

Cell culture models are a popular *in vitro* testing method to model complex systems which are inaccessible for such studies [42]. Additionally, physicochemical characterization of nanoparticles in biological fluids is popular for determining interactions between nanoparticles and biomolecules [43]. As a result of such studies, the biomolecule layer on a nanoparticle surface has been identified, and named the protein corona [43, 44].

1.2 Protein coronas on nanoparticle surfaces

When nanoparticles enter biological systems, they are immediately coated with a protein corona [43, 44]. The protein corona consists of proteins, ions, lipids, and other biomolecules which mask the identity of the nanoparticle [45]. As a result, the protein corona interacts with the cells and tissues in the human body rather than the nanoparticle [46, 47]. As such, understanding the identity of the protein corona is crucial to assess human health risks associated with nanoparticle exposure [48, 49], as well as the safety and efficacy of drug-delivery vehicles [32, 46, 50, 51].

Recently, it has been established that the protein corona is made up of two parts: the “soft” and the “hard” coronas [52, 53]. The soft corona is comprised of abundant, low affinity proteins whereas the hard corona is comprised of sparse, high affinity proteins [50]. The protein corona varies in protein composition and quantity based on physicochemical properties of the particles and the biological fluid into which the particles enter [54, 55]. Properties of the nanoparticle surface such as the degree of hydrophilicity can promote the adsorption of specific proteins over others. Other factors include the curvature of the nanoparticle surface, influenced by nanoparticle size, and the surface charge of the nanoparticle [49]. The nanoparticle surface can be altered, such as via the use of targeting ligands to improve trafficking to desired sites; however, if these ligands do not mitigate corona formation, that effect is diminished [56, 57].

Protein adsorption to the nanoparticle surface may influence the structure and function of adsorbed proteins, as well as affect the targeting of nanoparticles to biological components. Serum albumins are the most abundant protein in the blood, and as the cardiovascular system is spread throughout the entire body, these make good model proteins. One such serum albumin is bovine serum albumin which is 98% similar to the human analog, but much cheaper [58]. BSA has been widely characterized and studied in protein-substrate interactions. The structure of BSA is known to change as a function of pH [59, 60]. At acidic conditions near the isoelectric point, BSA begins to unfold. In acidic conditions, further from the isoelectric point, BSA assumes an extended structure, becoming almost linear rather than in the native heart shape. In basic conditions, BSA becomes more compact than its native structure. These changes have the potential to affect the proper function of BSA, such as if BSA adsorbed on a nanoparticle surface and carried out of the blood stream to a new pH environment, or if BSA assumed a new structure when adsorbed to the nanoparticle surface.

Corona characterization has been completed using a variety of methods to test different aspects of nanoparticle-protein interactions. One of the most common techniques for assessing protein corona formation onto nanoparticle surfaces is Fourier transform infrared (FTIR) spectroscopy. Various forms of this exist, and attenuated total reflectance (ATR) is the most common today. ATR-FTIR allows for real-time *in situ* analysis of protein adsorption onto nanoparticle surfaces without perturbing the interface [61-65]. The resulting spectra from ATR-FTIR can be processed to obtain more information, such as the subsequent protein structure after adsorption.

In addition to ATR-FTIR, quantifying the protein corona based on protein quantity and protein identity can be done using thermal gravimetric analysis (TGA) or proteomics, respectively

[51, 63]. These techniques build upon the information obtained from ATR-FTIR to provide a better idea of the proteins in the protein corona on nanoparticles.

1.3 Nanoparticle characterization

The physicochemical properties of nanoparticles affect their behavior, both for their intended purposes and for human health responses. For example, crystalline silicon dioxide has long been accepted as toxic, but the toxicity of amorphous silicon dioxide particles is still under debate [66]. Furthermore, which proteins are attracted to the nanoparticle to form the protein corona vary based on the properties at the nanoparticle surface, including hydrophilicity [67-69] and net charge [70, 71]. These properties are inherent to the nanoparticle, but can also be mediated through surface functionalization [51, 72], or through adsorption of solution components [73]. There are countless forms of silicon dioxide nanoparticles even among just amorphous silicon dioxide. Mesoporous nano-silicon dioxide are used for drug delivery systems and commonly have surface functionalization to improve targeting [72].

The size, shape, and surface charge of the nanoparticle itself governs interactions in aqueous media [20]. Proteins exhibit different affinity towards hydrophobic and hydrophilic surfaces [58, 67, 68, 74, 75]. For non-functionalized silica nanoparticles, the surface oxygen groups provide a hydrophilic-like surface in the presence of water [76]. These groups provide potential hydrogen binding sites with the protein at close distances from the nanoparticle surface [77]. Furthermore, although nanoparticle surfaces are often thought of as smooth, flat surfaces, this is not the case. The surface curvature of nanoparticles changes strongly as a function of nanoparticle diameter, and this angle can affect nanoparticle-protein interactions [78]. Finally, metal oxide nanoparticles may contain impurities and/or multiple crystalline forms [79]. This is not a concern for the silica nanoparticles of interest, but should be addressed for other

nanoparticles. Therefore, an understanding of nanoparticle size, both primary and aggregate, shape, charge, and composition are necessary to properly analyze a system.

1.4 Protein adsorption onto nanoparticle surfaces

The use of IR for determining protein structure was first identified in the 1950s. Since then, IR has become an increasingly popular tool for assessing protein structure on nanoparticle surfaces and investigating protein adsorption in real time. Proteins exhibit major bands in the IR spectrum due to the repeated nature of the amino acid backbone. These include the amide I, II, and III bands at 1600-1700, 1500-1600, and 1200-1350 cm^{-1}, respectively. The contributing motions to these bands are summarized in Table 1-1. Su, et al. investigated the adsorption of BSA onto a hydrophilic silicon dioxide/water interface near the isoelectric point [80]. Findings showed that at or near the isoelectric point of BSA, there was a surface excess of protein. However, moving away from the isoelectric point quickly decreased the amount of protein at the surface. Similar studies were completed by Wiśniewska, et al. and Fukuzaki, et al. with similar findings [81, 82].

Table 1-1. Characteristic IR vibrational modes for proteins [62, 65, 83, 84].

Region	Vibrational Frequency (cm^{-1})	Vibrational Mode
Amide I	1600-1700	$\nu_s(C=O)^{major}$, $\nu_s(C-N)^{minor}$
Amide II	1500-1600	$\nu_s(C-N)$, $\delta(N-H)^{out\ of\ phase}$, $\nu_s(C-C)^{minor}$
Amide III	1200-1350	$\nu_s(C-N)$, $\delta(N-H)^{in\ phase}$
Amide A	~3300	$\nu_s(NH)$
Amide B	~3100	$\nu_s(NH)$

ν_s symmetric stretching motion
δ bending mothing

To improve the understanding of protein adsorption, several studies have been conducted with individual amino acids at different pH values [62, 85]. These studies elucidate known charge on the analyte (the amino acid) and highlight differences that occur in adsorption including amino acid orientation on the surface and adsorbed amino acid structure as a function of pH. For dissolved

L-lysine adsorbed to the silicon dioxide nanoparticle surface, no significant shifts in the IR spectra were noted, indicating that the amino acid structure remained stable in the adsorbed state. Furthermore, mono-cationic lysine ($lysine^{1+}$) had the greatest adsorption to the silicon dioxide surface compared with di-cationic lysine, zwitterionic lysine, and anionic lysine [85]. This can be attributed to a negatively charged nanoparticle surface and charge-dependent interactions. Another study of lysine on silicon dioxide nanoparticles, largely based on solid-state NMR techniques, determined hydrogen bonding was the dominating interactive force between nanoparticle and amino acid, and that the structure of lysine is not necessarily maintained for all charged states [86]. These studies may aide in the understanding of BSA adsorption to the silicon dioxide surface as lysine is the third-most common amino acid present in BSA [87].

1.5 *In vitro* studies with nanoparticles and lung cells

Many studies have focused on adverse health effects with cell models *in vitro*. A549 cells, human adenocarcinoma alveolar epithelial cells, are commonly chosen for these types of studies because they are a well-established cell line for toxicology studies [29, 88, 89]. Other cell lines which have been used extensively include RAW264.7 cells, which are mouse alveolar macrophages [90, 91], and NCI-H441 cells which are human lung adenocarcinoma [88, 92]. Nanoparticle size, shape, and composition have all been shown to have an effect on cellular responses to nanoparticle exposure [93-96]. A summary of observed cellular responses in A549 cells is outlined in Table 1-2.

Table 1-2. A summary of existing literature on amorphous silicon dioxide nanoparticles and lung cell studies including particle diameter, the cell lines used, and a summary of these observed effects.

Particle Diameter	Cell line(s)	Cellular Response	Ref
10 nm 80 nm	A549	↓ cell viability ↑ LDH, ROS, and membrane LPO ↑ GSH levels ↔ GR and GPx activity	[97]
5-15 nm	A549 NCI-H441 THP-1	↓ cell viability (THP-1 only) ↔ IL-1β, IL-6, IL-8, TNF-α	[88]
5-15 nm	A549 and THP-1 co-culture NCI-H441 and THP-1 co-culture	↔IL-6 (NCI-H441 co-culture) ↔ TNF-α (both co-cultures)	[88]
15 nm 46 nm	A549	↓cell viability ↑ LDH and GSH	[29]
16 nm 60 nm 104 nm	A549	↓cell viability ↑ micronuclei ↑(weakly) DNA damage, chromosome breakage, chromosome loss	[98]
25 nm 50 nm	16HBE A549	↓cell viability ↑ ROS generation ↑ IL-6, IL-8, IL-1β (A549, 25 nm, 24h) ↑ IL-6, IL-8 (16HBE, 25 and 50 nm, 24 and 48h)	[89]
50 nm	A549	↓ ATP in serum-free medium Morphological changes in serum-free medium	[99]

*Abbreviations used in this table: GSH- glutathione, GPx- glutathione peroxidase, GR- glutathione reductase, IL- interleukin, LDH- lactate dehydrogenase, LPO- lipid peroxidation, ROS- reactive oxygen species, TNF- tumor necrosis factor

**Cell lines used in this table: A549 human adenocarcinoma alveolar epithelial cells, 16HBE human bronchial epithelial cells, THP-1 alveolar macrophages, and NCI H411 human lung adenocarcinoma cells

A549 cells were used for the studies in this thesis, however, they are not necessarily the best model for lung uptake, and they certainly are not the only model that should be used. The greatest benefit for A549 cells is the extensive literature available on toxicity studies, as previewed in Table 1-2. However, the cancerous nature of the cells makes them a poor model for healthy individuals. Additionally, the alveolar region is just one region in the lungs in which inhaled

nanoparticles may deposit. There are multiple bronchial cell lines, such as 16HBE cells, which can be used to investigate a different region of the lungs. Furthermore, certain toxic responses cannot be investigated in A549 cells accurately, such as cytokine release, as this is mediated *in vivo* by macrophages.

1.6 Objectives

This thesis aims to improve the understanding of the nanoparticle-protein interactions between a hydrophilic, fumed silica nanoparticle approved for food and pharmaceutical use and a model protein. Crystalline silica is known to be toxic, but amorphous silica is believed to be non-toxic. Even so, amorphous silica takes on many forms and the surface of these particles is easily functionalized for specific uses. The future of silica in bionanotechnology is promising, and therefore necessary studies on the nature of the silica surface in the presence of biological models and behavior *in vitro* provide necessary information towards the safety and efficacy of these particles. The objectives for achieving this are as follows:

Objective 1: Characterize the BSA protein corona on silica nanoparticles in terms of surface coverage and protein structure as a function of pH.

Objective 2: Characterize the BSA protein corona on silica nanoparticles in terms of surface coverage and interparticle interactions as a function of solution ions.

Objective 3: Evaluate the cytotoxic response of BSA-coated and uncoated silica nanoparticles in a model lung cell line.

Chapter 2 The effect of pH on the protein corona

2.1 Introduction

Nanoparticles that enter the human body are immediately coated with a layer of biomolecules, known as the protein corona [43, 44]. This corona may vary based on the conditions of the aqueous environment surrounding the nanoparticle [81], as well as the physicochemical nature of the nanoparticle surface [67, 68]. As silica nanoparticles are used for a variety of applications including in food additives, cosmetics, and pharmaceuticals, the method of internalization and thus the target organ varies based on application [29, 30, 100].

Although most of the human body is at pH 7.4, several organs operate at very different pH values. For example, the stomach is highly acidic with pH 2.0, whereas the pH is closer to 8.0 in the gastrointestinal tract [101]. There has been some research that the pH of the alveolar sacs in the lungs are more acidic with a pH of about 4.5 [102]. Therefore, investigating the protein corona as a function of pH is critical when determined the safety and efficacy of silica nanoparticles for consumer products.

Conducting a study in real biological fluids is difficult as there are many molecules which compete for binding sites on a nanoparticle surface, and the dynamic nature of the protein corona creates much variability in the precise composition at any time [52]. Furthermore, analyzing which protein or ion is adsorbed to the surface is difficult without trained scientists and expensive techniques [45, 103, 104]. Thus, a model protein can be used to investigate the nature of the protein corona in a simple aqueous medium to develop an understanding about the overall nature of the protein corona.

In these studies, the model protein bovine serum albumin was chosen for its biological relevance and abundance in the blood stream. Serum albumins constitute more than half the proteins in the blood and are ubiquitous in biological fluids [58]. Serum albumins function mainly as transporter proteins to carry molecules from one location to another through the blood. The bovine serum albumin is 98% similar to the human analog and cheaper, making it a popular choice for laboratory studies. Serum albumins have been widely studied and characterized, and they are known to undergo conformational changes as a function of pH [105, 106]. Thus, the expected structure of free BSA at different pH values can be used to analyze conformational changes upon adsorption to the silica nanoparticle surface.

2.2 Materials and methods

Silica nanoparticles, CAB-O-SIL® HS-5, were gifted from the Cabot Corporation and used with no further processing. These hydrophilic, fumed silica powders have been approved for adhesives, coatings, food additives, pharmaceuticals, skin and beauty care products, among other uses as listed by the company. The primary particle size of these particles was determined using transmission electron microscopy (TEM, JEOL JEM-1230) and ImageJ software. A 100 μg/mL solution of silica nanoparticles in isopropanol was prepared and sonicated at 40% amplitude for 10 minutes, in 20 seconds on and 10 seconds off intervals. A single drop of this suspension was added to a Formvar-backed copper coated TEM grid and dried overnight. The specific surface area of these particles was confirmed against company specifications using the seven-point nitrogen adsorption isotherm BET analysis (Quantachrome BET Nova 4200e) using the average of three independent trials.

Aggregation in aqueous media and the zeta potential were determined for these particles in water. Pure Optima® water (Fisher Chemical) was adjusted to the desired pH using 1M

hydrochloric acid (HCl, Fisher Scientific, certified ACS plus) or 0.8M sodium hydroxide (NaOH, Fisher Scientific, certified ACS plus). Nanoparticle suspensions of 5 mg/mL silica in water were sonicated in a water bath sonicator for 20 minutes before being stored overnight at 4ºC for 24-hours prior to analysis. A protein corona was created on the nanoparticle surface by mixing 5 mg/mL silica nanoparticles with 1 mg/mL BSA (>96% purity, Sigma-Aldrich) solution. These solutions were sonicated and stored under the same conditions. Immediately before dynamic light scattering (DLS) and laser Doppler velocimetry (Beckman-Coulter Delsa Nano C) suspensions were sonicated for 10 minutes in a water bath sonicator. Measurements in the presence and absence of BSA were compared. Samples were run in triplicate and conditions were duplicated to ensure reproducibility.

Thermogravimetric analysis (TGA, Pyris 1 TGA, Perkin-Elmer) was used to quantify BSA adsorption onto silica nanoparticles. Suspensions of 4 mg silica in 1 mL of 1 mg/mL BSA solution in were sonicated for 20 minutes and then incubated at 4ºC for 24 hours. Samples were centrifuged at 2,500 rpm to form a pellet, the supernatant was removed, nanoparticles were suspended in water, and samples were washed twice in this manner before drying partially covered in a chemical fume hood for two days. Once completely dry, samples were heated at 5°C/minute from room temperature to 700°C under a flow of air. Any mass loss at or below the boiling point of water was assumed to be free water. Any mass loss above the boiling point of water was assumed protein.

Attenuated total reflectance Fourier Transform infrared (ATR-FTIR) spectroscopy was used for real-time *in situ* observation of protein adsorption onto the silica nanoparticle surface (Nicolet Nexus Spectrometer, Thermo Nicolet Corporation). Before experimental conditions were determined, a series of tests with a nanoparticle thin film and Optima® water in a horizontal flow cell were conducted. The purpose of these experiments was to obtain the maximum time frame for

experiments, without losing too much of the nanoparticle surface. The optimal experimental design follows in the next paragraph.

First, a spectrum of the AMTIR crystal element (PIKE Technologies) was obtained. Then, a thin-film nanoparticle suspension was prepared using 8 mg silica nanoparticles in 1 mL Optima® water. This was sonicated in a bath sonicator for five minutes and added to the AMTIR crystal in an even layer. This layer was allowed to dry completely overnight before adding protein solution. The spectrum of the dried nanoparticle thin-film was obtained. Then, a horizontal flow cell was attached and Optima® water fed through to obtain a spectrum of the wet nanoparticle surface for subtraction in spectral processing. A 1 mg/mL solution of BSA passed through the flow cell at ~1 mL/minute for 90 minutes. Spectra were collected every 10 minutes during this time. Finally, pure Optima® water, without any protein, was added to the flow cell for 60 minutes to determine whether adsorption was reversible or irreversible. Absorbance spectra were obtained by subtracting the wet nanoparticle film from each spectrum of BSA on the nanoparticle surface. This yields the absorbance of BSA, but includes any water bound within the protein.

Curve fitting of the ATR-FTIR spectra was completed in Casa XPS using five component bands in the amide I region and a Gaussian-Lorentzian shape. The curve fit spectra were further modified to have a linear baseline at zero in the amide I region, and a peak maximum of exactly one absorbance unit in the amide I region.

2.3 Nanoparticle characterization

The results from TEM and ImageJ indicate that silica nanoparticles were 14 ± 2 nm in diameter for the primary size (Figure 2-1). However, they were obtained in fused aggregates of 200 – 300 nm. The specific surface area for these particles was 330 ± 24 m^2/g. The relationship between primary particle size and specific surface area can be done mathematically [62], and

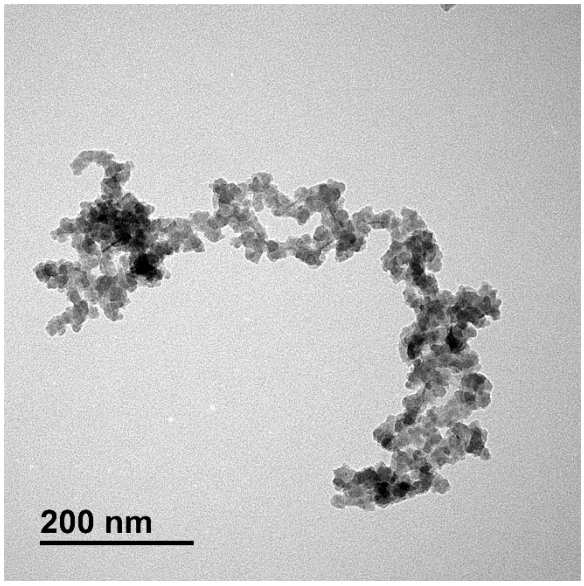

Figure 2-1. TEM of silica nanoparticles suspended in isopropanol

reveal that for 14 nm particles, the specific surface area should be about 194 m^2/g. This is much lower than both the experimental data and company specifications, and suggests that the pores generated by fused particles enhances the available surface area. Thus, the binding of protein to these nanoparticle surfaces may behave more like mesoporous silica than other non-fumed, non-porous silica samples to a degree.

A background spectrum for silica nanoparticles was obtained using ATR-FTIR spectroscopy. This spectrum reveals the characteristic peaks for silica nanoparticles in the IR region (Figure 2-2). Peak locations are characteristic of nano-silica due to silicon-oxygen interactions.

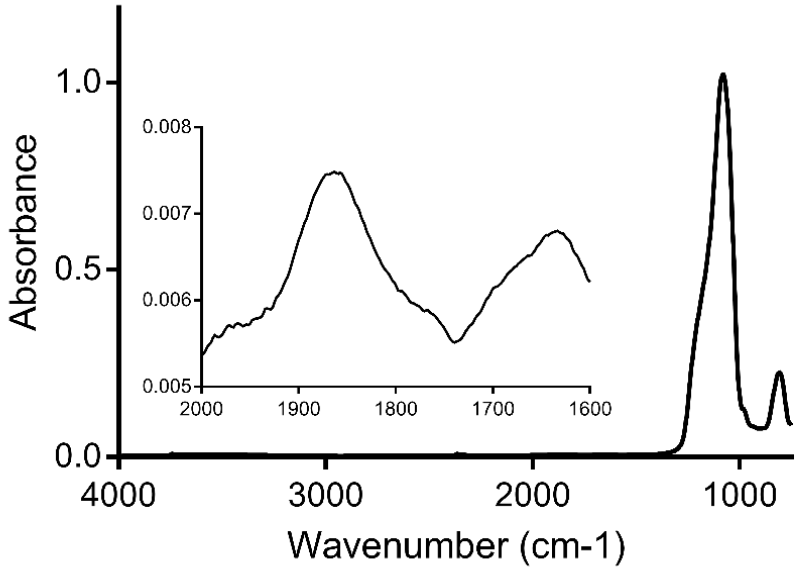

Figure 2-2. ATR-FTIR thin film spectrum of dried silica

2.4 Hydrodynamic diameter and zeta potential in aqueous media

We hypothesized that protein adsorption onto the nanoparticle surface would vary as a function of pH, based on previous studies within the Grassian group and the existing literature [20, 22, 62, 81, 107]. Silica nanoparticles with and without BSA coating were suspended in pure water, pH-adjusted to the desired values. These solutions were analyzed for aggregate formation and zeta potential, to determine the effects of both BSA and of changing pH values. Adsorbed BSA will alter the zeta potential of bare silica nanoparticles by bringing it closer to the zeta potential of BSA at that pH. Thus, differences between the zeta potential provides information on protein adsorption. The hydrodynamic diameter was measured to assess aggregation (Figure 2-3) and the zeta potential was measured to assess adsorption and net charge on particles (Figure 2-4).

Results from a two-way ANOVA comparing the pristine particles to the BSA-coated particles revealed significant differences in aggregation for the pH values of: 3.0, 3.7, and 4.7, which is consistent with known isoelectric points. The isoelectric point of hydrophilic, fumed silica

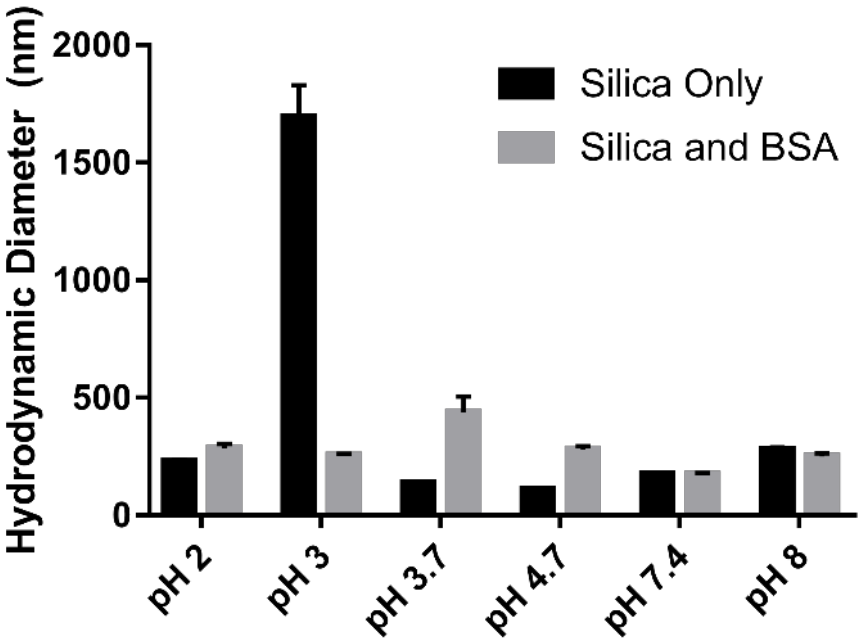

Figure 2-3. Hydrodynamic diameter of nanoparticles in the presence and absence of BSA. Data is presented as the average of three trials with standard deviation.

is between pH 2 and pH 3 [108], and the isoelectric point of BSA occurs at pH 4.7 [81, 109]. The isoelectric point of the BSA-silica complex, determined experimentally, occurs between these two pH values. The tendency for particles to agglomerate in solution is largely driven by electrostatic interactions. This is confirmed with the large aggregate diameters occurring near known isoelectric points. The two-way ANOVA test for silica with or without BSA revealed that the increase in hydrodynamic diameter in the presence of BSA at pH 3.7 is significant to all other measurements in the presence of BSA. Furthermore, all other comparisons in the presence of BSA show no significance. Nanoparticle aggregation in aqueous media presents difficulties with keeping

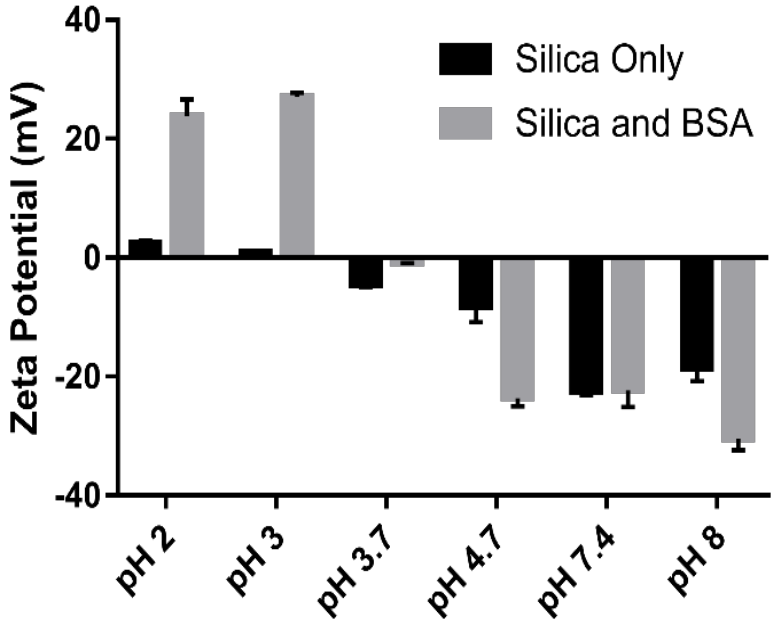

Figure 2-4. Zeta potential of nanoparticles in the presence and absence of BSA. Data is presented as the average of three trials with standard deviation.

particles suspended, as heavier particles are affected more readily by gravitational forces, and with proper dosing and delivery of particles *in vitro* and *in vivo*.

Research has shown that the net charge a particle carries affects its interactions with cells. Specifically, charged particles show greater toxicity than neutral particles and positively charged nanoparticles are more cytotoxic than their negatively charged variants [71, 110]. Thus, understanding the charge that particles carry is important for assessing their potential for cellular uptake and subsequent toxicity. The zeta potential for these particles varies as a function of pH as expected, above the isoelectric point, the zeta potential is negative and below the isoelectric point, the zeta potential is positive.

At pH 7.4, the zeta potential for silica nanoparticles in the presence or absence of BSA is almost the same. This cannot provide additional information on BSA adsorption to the surface, but it does suggest that there is good electrostatic repulsion in the system to avoid unwanted

aggregation. This is further supported by the similar hydrodynamic diameter, which is about the diameter of the fused aggregates for native silica. At the remaining pH values, BSA is adsorbing to the nanoparticle surface because the surface charge is closer to what is expected for free BSA than uncoated silica. Unfortunately, BSA monomers are beyond the detection limit of the instrument so this information must be extrapolated using the known isoelectric point of BSA. Protein adsorption to the nanoparticle surface was also assessed using spectroscopy.

2.5 Real-time protein adsorption to the nanoparticle surface

Protein adsorption onto the silica nanoparticle surface was investigated as a function of time and pH. The reversibility of adsorption was also investigated by removing additional protein from the flow system, and determining if protein was removed from the nanoparticle surface as a result.

Determining the optimum time for experiments was necessary for these nanoparticles. The limitations on flow rate and time were determined experimentally using trial and error. For these silica nanoparticles, their adsorption to the AMTIR crystal was not strong enough for prolonged studies as have been reported in the literature [51, 62]. When the nanoparticle surface is coated with proteins a sharp negative peak characteristic of the nanoparticle surface may occur. However, this peak may also arise from the desorption of nanoparticles from the surface. Therefore, to determine if this observed peak was due to protein binding or due to nanoparticle desorption, pure water with no pH adjustment was run through the flow system until the negative peak was observed. From repeated experiments, it was determined that a maximum time of three hours could be used for experimental studies, without losing the silica nanoparticle thin film.

Spectra for free BSA (10 mg/mL) were obtained to determine the expected IR peak locations in the absence of conformational change (Figure 2-5). Both the overall intensity and the peak positions remain relatively constant in the solution phase, suggesting that conformational changes occur more slowly than the experimental process. The observed peaks arise from the repeated nature of the amino acid backbone of the protein, and were summarized in Table 1-1. An additional peak between 1700 and 1720 cm^{-1} arises when the carboxylic acid groups of the amino acid sequence are protonated, such as at low pH values. This is not observable for the concentration of BSA provided in the solution phase.

Upon adsorption to the nanoparticle surface, the intensity of the signal from the protein increases. This lowers the minimum protein concentration necessary to achieve detectable absorbance. A 1 mg/mL BSA solution was flowed over the nanoparticle thin film for one and a half hours. Spectra were collected every 10 minutes to visualize the real-time adsorption of BSA in terms of quantity (absorbance intensity) and conformation (peak locations). Select spectra are shown at each pH, with peak positions labeled consistently with the free BSA spectra (Figure 2-6).

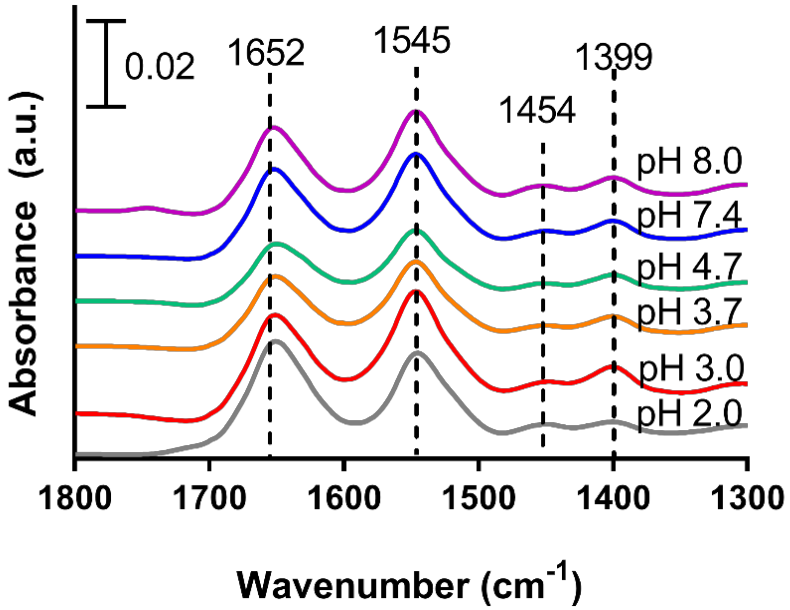

Figure 2-5. ATR-FTIR spectra for 10 mg/mL BSA in pH-adjusted water

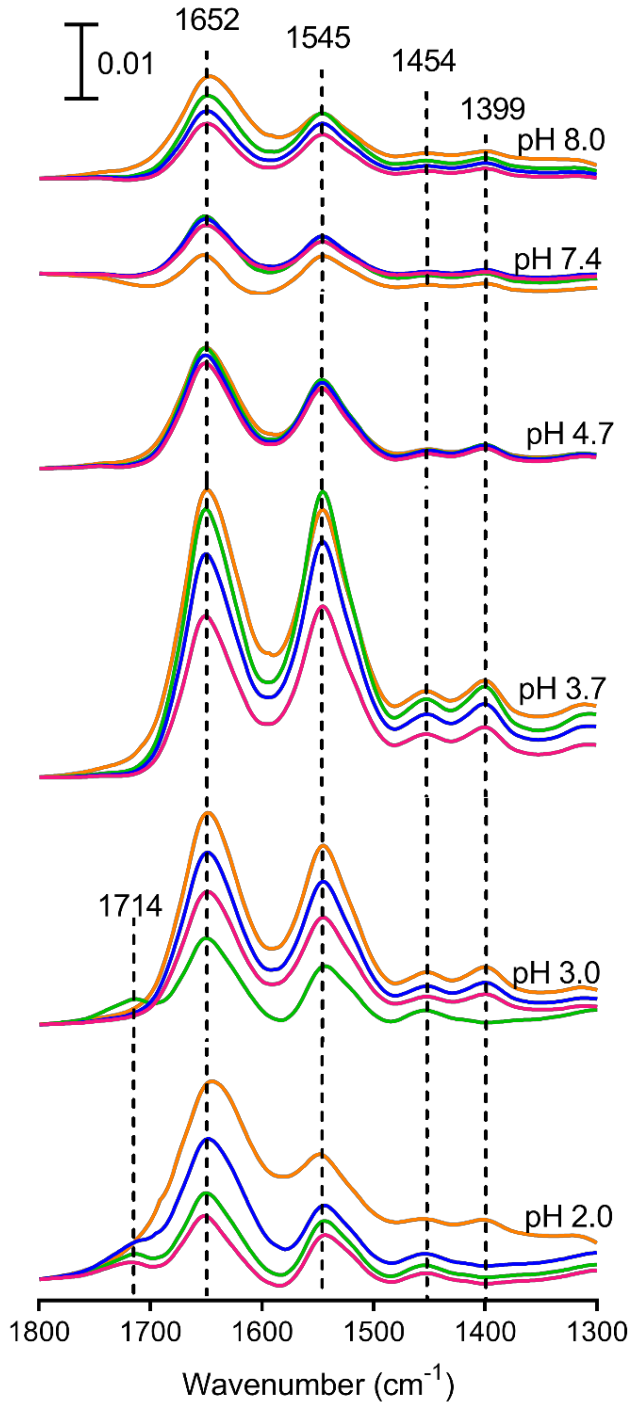

Figure 2-6. ATR-FTIR spectra for 1 mg/mL BSA adsorbed onto the silica nanoparticle surface as a function of pH. Labeled peak locations are from the solution phase BSA, and spectra for each pH are given at 30 minutes (pink), 60 minutes (blue), 90 minutes (green), and 160 minutes (orange).

An additional peak appears at 1714 cm^{-1} immediately at pH 2 and over time at pH 3 arises from the protonated carboxylic acid groups in the amino acid backbone.

Peak shifts will occur in the event of changes in protein structure [111]. For both the solution phase and the adsorbed phase BSA, peak shifts are less than 5 cm^{-1} in either direction from the free BSA at neutral pH. This indicates that BSA does not undergo structural deformations upon adsorption to the silica nanoparticle surface.

For each pH, spectra are shown for 30 minutes (pink), 60 minutes (blue), 90 minutes (green), and 160 minutes (orange), which is 1-hour of desorption. At many of the chosen pH values, the final time point has a greater absorbance intensity than the final addition of BSA to the flow system. This phenomenon arises from protein structure rearrangement on the nanoparticle surface, specifically in the intermolecular hydrogen bonds [77]. The magnitude of this effect is greatest for pH 2 and pH 3, suggesting that the increase in pH between the adsorption and desorption phase causes more rearrangement when the difference between pH is greater.

Although the general trend is for absorbance intensity to increase over time, as more BSA adsorbs to the silica nanoparticle surface, this is not always the case. For example, at pH 4.7, BSA adsorbs to the silica surface quickly and there is little change in absorbance intensity after 10 minutes. The same effect is observed at pH 7.4, however, at pH 7.4 BSA desorbs from the nanoparticle surface. This difference in desorption is important when assessing the reversibility of protein adsorption, however, without also understanding the protein secondary structure, retained protein function cannot be assumed. The strong relationship between intermolecular bonds and absorbance intensity in this case makes it difficult, if not impossible, to quantify adsorbed protein from ATR-FTIR alone, and therefore TGA has been used for quantitative analyses.

2.6 Changes in adsorbed protein structure

The spectra obtained from ATR-FTIR spectroscopy were used to obtain information on the secondary structure of adsorbed and free protein. The amide I peak was fit to five-component bands characteristic of protein secondary structure [67, 68, 112]. The effects of both pH and adsorption on the protein secondary structure were investigated. In Figure 2-7, the spectra for free BSA and adsorbed BSA have been plotted side by side for each pH value. Statistical analysis comparing both pH and adsorption reveal no significant changes in proteins structure occur in this system. Thus, adsorption to the silica nanoparticle surface does not affect the secondary structure of BSA.

Upon adsorption to the nanoparticle surface, BSA is expected to lose most of its secondary structure in the alpha helices [67, 68]. Comparing the solution phase to the adsorbed phase after 90 minutes, alpha helix content only decreases upon adsorption at pH 2.0. However, the alpha helix content does change as a function of time and pH (Figure 2-8). In most cases, pure water in the desorption phase of the study increases the solution pH. Increasing the pH from acidic to basic conditions is expected to increase the alpha helix content as BSA should return to its native conformation. This occurs for pH 2.0, but not for any other acidic pH. The pH of pure water is slightly lower than neutral pH, and therefore the values of pH 7.4 and 8.0 experience a decrease in pH upon switching to a pure-water system. Although a small decrease in alpha helix content is observed at pH 7.4, the alpha helix content over time is still relatively constant. The most consistent

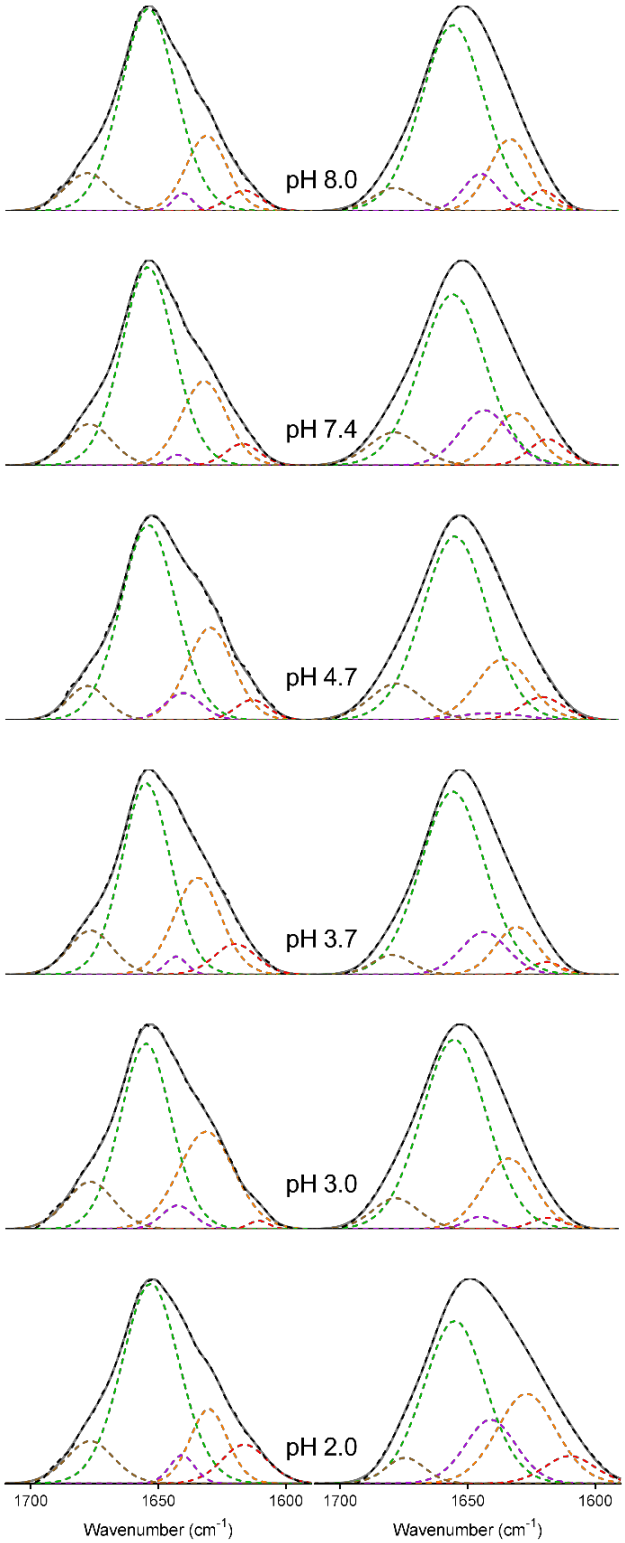

Figure 2-7. Amide I band curve fitting for protein secondary structure with five components: beta sheet or beta turn (brown, dotted), alpha helix (green, dotted), random chains (purple, dotted), extended chains or beta sheets (orange, dotted), and side chain moieties (red, dotted). Additional lines shown for baseline (black, solid) and original spectra (black, dotted), as well as the overall fit (gray, solid) for the solution phase (left) and the adsorbed phase (right).

alpha helix content over all pH values occurs at pH 3.7. At this pH, the alpha helix content fluctuates slightly as a function of time, but the overall change is less than 5%.

The secondary structure of bovine serum albumin adsorbed to the silica nanoparticle surface varies more as a function of adsorption than as a function of pH. This is promising news for the potential use of silica nanoparticles as drug delivery carriers, as the protein corona may be able to withstand a wide variety of pH values *in vivo*. However, the loss of available protein to carry out basic biological processes is also a concern.

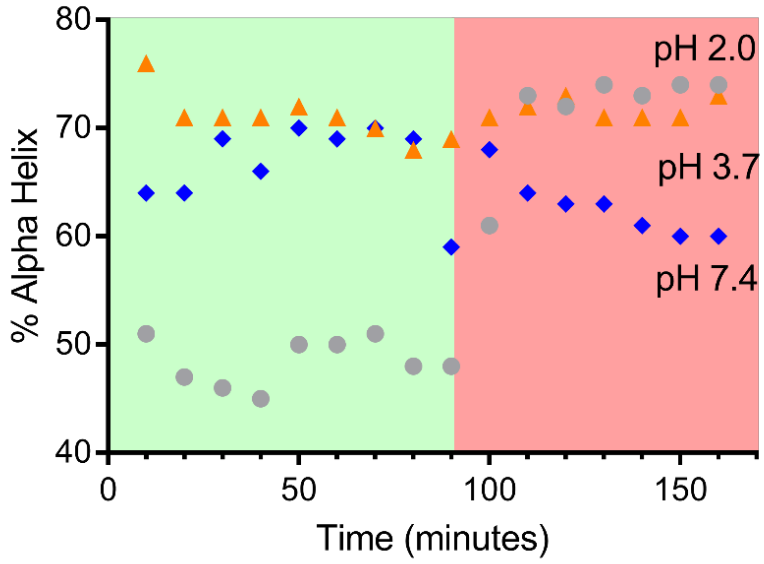

Figure 2-8. Alpha helix content at select pH highlighting the changes over time for adsorption (green) and desorption (red).

2.7 Quantitative analysis of protein adsorption to nanoparticle surfaces

Thermogravimetric analysis is a useful mass-based tool for assessing changing in sample composition. The temperature of vaporization differs for different molecules, and therefore the temperature of mass loss can be connected to the components present in the system. Water boils at 100ºC, therefore any mass loss below 100ºC is free water. Unbound BSA protein vaporizes between 400-500ºC, whereas bound BSA vaporizes at slightly higher temperatures. Thus, any additional mass lost below 600ºC is protein. Using the initial mass, mass after water loss, and mass

after protein loss, the amount of silica nanoparticles present can be determined. Then, this mass is combined with the BET specific surface area measured experimentally to obtain the surface area onto which the BSA was bound. Presenting the data as molecules of protein per surface area of nanoparticles allows for normalization across different runs at the same and at different pH values.

These data (Figure 2-9) revealed that the most BSA binds at pH 3.7, which is consistent with the results obtained from ATR-FTIR spectroscopy. Second and third to this are BSA bound at pH 3.0 and pH 4.7, which are in line with the literature assumption that the most protein binds at either the protein or the substrate isoelectric point. A one-way ANOVA was conducted to determine whether the differences in adsorbed protein were statistically significant. Only the difference between adsorption at pH 2.0 and pH 3.0 returned significant values. This is likely due to the large error bar at pH 3.7.

An additional set of measurements were taken at pH 3.7 to determine if the error could be reduced by increasing the number of samples. Results were that the error could not be decreased

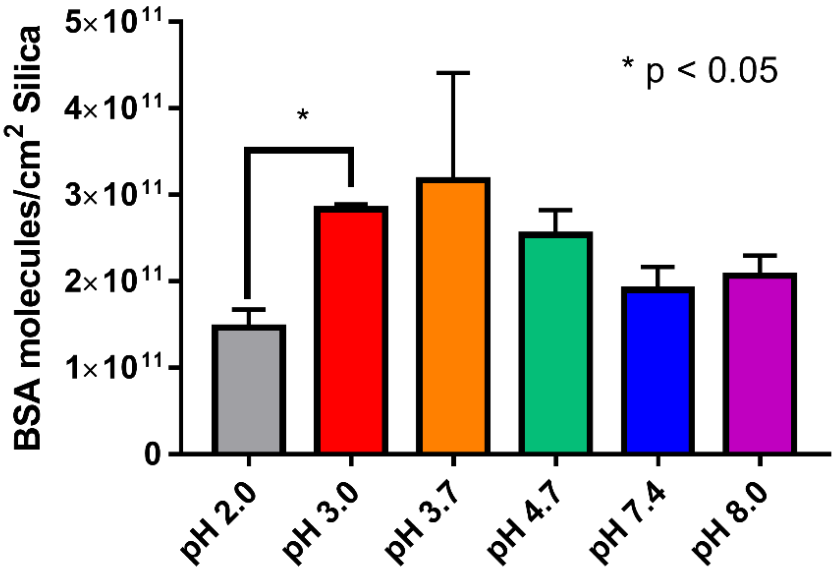

Figure 2-9. Adsorbed BSA on the silica nanoparticle surface in units of BSA molecules per surface area of silica nanoparticles.

nor increased by increasing the number of trials. Therefore, it may be reasonable to assume that the kinetics of BSA adsorption to the silica nanoparticle surface are altered as a function of pH, and the time necessary to obtain a uniform protein corona is not the same for all conditions.

The maximum adsorption of protein to the nanoparticle surface is expected to occur at an isoelectric point. This could be the isoelectric point of the substrate [82, 113], or the protein [81, 107]. However, these results indicated that the maximum adsorption occurs at the isoelectric point of the complex for the nanoparticle-protein system. This may be different in buffered and/or saline solutions, as ions can alter the surface characteristics of the nanoparticles and influence protein adsorption [73].

2.8 Conclusion

These studies determined that the silica nanoparticle-bovine serum albumin protein corona is narrowly influenced by changing pH values. Changing pH values impacts aggregation at the isoelectric point and the zeta potential of the silica nanoparticles in the presence and absence of BSA. It is possible that pH also influences the kinetics driving protein binding to the nanoparticle surface.

The quantity of BSA adsorbed to the silica nanoparticle surface varies as a function of pH, with the least BSA adsorbing at pH 2.0 and the greatest BSA adsorption at the silica-BSA complex isoelectric point of pH 3.7. The maximum adsorption is consistent with absorbance intensity in ATR-FTIR spectra, however, the lowest absorbance intensity occurred for pH 7.4 rather than pH 2.0. This may be a result of protein rearrangement on the nanoparticle surface affecting the absorbance intensity.

The secondary structure of BSA changes slightly between the free BSA and the adsorbed BSA, with the greatest observed changes in the random chains. The greatest change is expected to be in the alpha helix content, and pH 2.0 exhibited the largest decrease. However, for most pH values, the greatest change is in the beta structures rather than the alpha helices. This is common for other protein types, but not BSA.

Although these results are highly informative for *in vitro* and *in vivo* administration of silica nanoparticles for tests regarding food and pharmaceutical safety, the relevance to the human body is lacking. Pure water does not exist biologically, and therefore studies with ionic solutions must be done to improve the biological relevance of these experiments. Furthermore, a recent study of BSA adsorption onto surface-functionalize mesoporous silica for drug delivery applications in cell culture media reported that only 10% alpha helix structure remained upon adsorption [51]. Therefore, evidence exists that the observed responses of BSA are influenced by the solution components and the nanoparticle substrate. Further studies presented in this thesis investigate other media and substrates in addition to water to begin to tease out the driving forces for these effects.

This chapter was formatted based on the following publication: Givens, B.E., et al, *Adsorption of bovine serum albumin on silicon dioxide nanoparticles: Impact of pH on nanoparticle-protein interactions*. Biointerphases, 2017. **12**(2): DOI: 10.1116/1.4982598

Chapter 3 The effect of pH and nanoparticle substrate on protein corona formation

3.1 Introduction

Among the most prevalent metal oxides are titanium dioxide (TiO_2) and silicon dioxide (silica) [6, 114]. Both nanoparticles are critical materials in pigments and are used as food additives [26, 29, 30, 115-117]. Despite their benefits to these industries, there is evidence showing that internalized nanoparticles are harmful towards human health [118, 119]. Furthermore, protein adsorption from the body to the nanoparticle surface may result in protein denaturation and subsequently loss of protein function [67].

The protein corona that forms on the nanoparticle surface changes as a function of pH, as demonstrated in Chapter 2. However, this corona also be substrate-dependent. Therefore, studies were done at two pH values, pH 7.4, the physiological pH, and pH 2.0, the pH in the stomach to aide in digestion, with TiO_2 and silica nanoparticles. Additionally, these pH values highlight two distinct conformations of BSA, the normal form and the extended form. In these forms, BSA measures $8.0 \times 8.0 \times 3.0$ Å or $2.1 \times 2.1 \times 25.0$ Å, respectively [105, 106].

In order to monitor protein adsorption and assess protein conformation, ATR-FTIR spectroscopy was used for real-time adsorption of BSA to each nanoparticle surface and the resulting spectra were further analyzed to obtain the secondary structure of BSA. During the ATR-FTIR experiments, saturation on the nanoparticle surface could not be obtained for silica nanoparticles, therefore, TGA was used to quantity BSA adsorption to the nanoparticle surfaces [111], rather than the Langmuir isotherm method which has been used previously with TiO_2 [62].

3.2 Materials and methods

The hydrophilic fumed silica nanoparticles, CAB-O-SIL® HS-5, were gifted from the Cabot Corporation and used with no further processing. TiO_2 nanoparticles were purchased from Sigma-Aldrich. The crystallinity of these nanoparticles was determined from powder x-ray diffraction (XRD, Bruker D8 Advance). TEM (JEOL JEM-1230) and ImageJ were used to obtain primary particle size. For TEM images, a 100 µg/mL solution of nanoparticles in isopropanol (silica) or ethanol (TiO_2) was prepared and sonicated for several minutes. These samples were deposited dropwise onto TEM copper grids and dried overnight before imaging. The specific surface area of the nanoparticles was determined using nitrogen adsorption with seven-point BET analysis (Quantachrome BET Nova 4200e). Nanoparticles were allowed to degas overnight at 300ºC prior to analysis. The average and standard deviation of three independent trials is reported.

Laser Doppler velocimetry (Beckman-Coulter Nano C and Zetasizer Nano ZS90) was used to determine the zeta potential as a function of pH for silica and TiO_2 nanoparticles. The zeta potential values were further used to calculate the isoelectric point by plotting the zeta potential as a function of pH and fitting this to a linear trend line. The pH value at which the trend line was equivalent to zero was then calculated. Samples were prepared by mixing 5 mg of silica or TiO_2 with 5 mL of Optima water and adjusted to the desired pH with 1 M HCL or 800 mM NaOH solution. Measurements in the presence and absence of 1 mg/mL of BSA (98% purity, Sigma-Aldrich) were obtained across a wide range of pHs, including those of interest at pH 2.0 and 7.4, in order to determine the isoelectric point as described above. Samples were run in triplicate and conditions were duplicated to ensure reliability.

The ATR-FTIR spectra for solution phase BSA at the pH values of interest were collected on a clean AMTIR crystal (PIKE Technologies) with a BSA concentration of 10 mg/mL. The

adsorption of BSA was measured on both nanoparticle surfaces by depositing a thin nanoparticle film of 2.5 mg TiO_2 in 1 mL Optima water or 8.0 mg silica in 1 mL Optima water. The nanoparticle suspension for these films were sonicated for 5 minutes to obtain a uniform mixture. After depositing on the AMTIR crystal element, the films were dried overnight. A horizontal flow cell (PIKE Technologies) was used to slowly flow (~1 mL/min) Optima water at the pH of interest above the nanoparticle thin film to remove loosely bound particles and to collect a background spectrum. Then a solution containing BSA (Sigma-Aldrich; 1 mg/mL; pH 2.0, pH 7.4) was introduced and a slow flow over the nanoparticle coated crystal was established while collecting spectra every ten minutes for one and a half hours.

Spectral processing was completed in the OMNIC™ Series Software (Thermo Fisher Scientific). Overall absorbance spectra were obtained by subtracting the water on nanoparticle film spectrum from each time-dependent spectrum of BSA adsorption. The resulting absorbance spectra were fit to a Gaussian-Lorentzian shape with five component bands in the amide I region. The initial guess for these five components was obtained from literature values [67, 112], and the fit for the solution phase BSA at each pH. All spectra were further processed to have a linear baseline at zero and a maximum peak height equal to 1.0 for direct comparisons across different conditions

Quantification of the protein adsorbed onto the nanoparticle surface was done through thermogravimetric analysis (TGA, Pyris 1 TGA, Perkin-Elmer). Triplicate trials were completed and averaged for each nanoparticle at each pH of interest. A 4 mg/mL solution of silica was prepared in 1 mg/mL BSA and a 2.5 mg/mL solution of TiO_2 was prepared in 1 mg/mL BSA. A total of 1 mL was prepared for each trial. Nanoparticles in protein solution were sonicated in a water bath sonicator for 20 minutes to ensure both nanoparticles and proteins were suspended, and

samples were then incubated at 4ºC overnight to coat the nanoparticles and prevent protein denaturation. Samples were then washed three times in pure water via centrifugation. Washed samples were allowed to dry partially covered in a fume hood for 2-3 days, or until water had visibly evaporated. Dried samples were crushed into a fine powder and placed on a platinum pan in as close to a single layer as possible, using the maximum amount of surface area for desorption. Samples were heated from room temperature to 700ºC at a rate of 5ºC per minute. The quantity of protein adsorbed to the nanoparticle surface was determined by calculating the mass of the protein lost from 100 – 600ºC and the initial mass of the nanoparticle loaded by subtracting the total mass loss from the initial mass.

All experiments on the TiO_2 substrate were prepared and conducted by Zhenzhu Xu.

3.3 Nanoparticle characterization

The primary size of the nanoparticles were 22 ± 1 nm for TiO_2, and 14 ± 2 nm for silica determined from TEM (Figure 3-1). The specific surface area for these particles was 50 ± 8 m^2/g

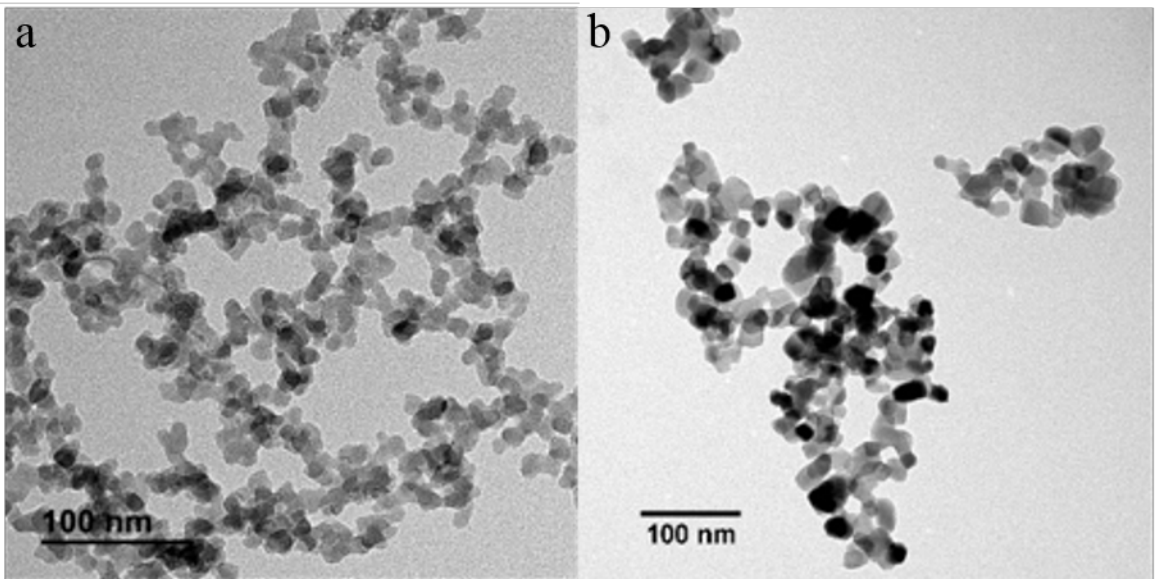

Figure 3-1. Transmission electron micrographs of a) silica nanoparticles and b) TiO_2 nanoparticles

and 330 ± 24 m^2/g for TiO_2 and silica, respectively. The phase state for TiO_2 nanoparticles was

determined from XRD, and the TiO_2 was 86% anatase and 14% rutile. The isoelectric point of these materials was determined using zeta potential values over a range of pH (Figure 3-2), and

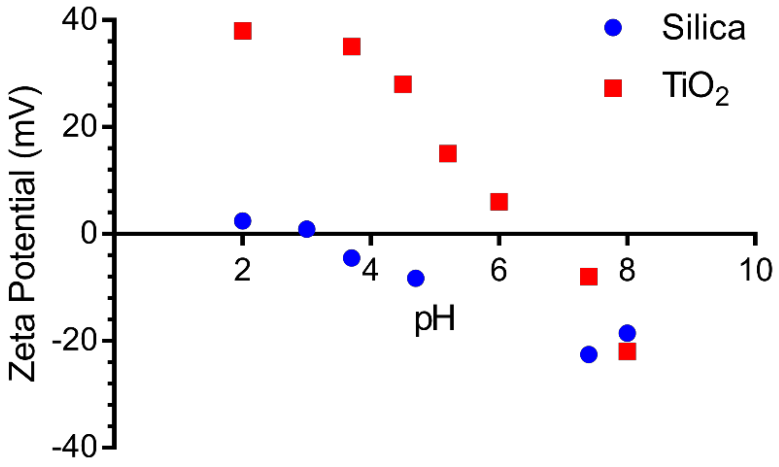

Figure 3-2. Zeta potential measurements from pH 2.0 to pH 8.0 for both silica and TiO_2 in water to determine the isoelectric point of each nanoparticle

occurred at pH 6.5 or pH 2.7 for TiO_2 and silica, respectively.

The experimental determination of the nanoparticle isoelectric point is useful in predicting differences in protein behavior on nanoparticle surfaces. Although there are literature reported isoelectric points of similar or the same nanoparticles [108, 113], the behavior of the specific lot of nanoparticle and the experimental conditions can alter this value [107]. Understanding that the isoelectric point of silica is in the acidic range, and the isoelectric point of TiO_2 is in the neutral range, suggests that protein adsorption will be greater on the two nanoparticle surfaces at different pH values.

3.4 ATR-FTIR monitoring of protein adsorption to the nanoparticle surfaces

The characteristic IR peaks for proteins are independent of the nanoparticle substrate (Table 1-1). However, the interactions between the nanoparticle and the protein may change, and can be visualized by peak shifts to different wavenumbers. The ATR-FTIR spectra for 10 mg/mL BSA in solution at pH 7.4 and pH 2.0 in the amide regions is presented in Figure 3-3 [61, 83, 84,

120, 121]. As compared with the spectrum at pH 7.4, the pH 2.0 spectrum contains an additional peak at 1712 cm^{-1} which corresponds to a carbonyl stretch associated with the protonation of COO^- groups in amino acids to form COOH [61, 62]. Additionally, the peak intensity of the 1399 cm^{-1} peak is greater at pH 7.4 than pH 2.0 due to the C-O carboxylate stretch of deprotonated amino acids [83].

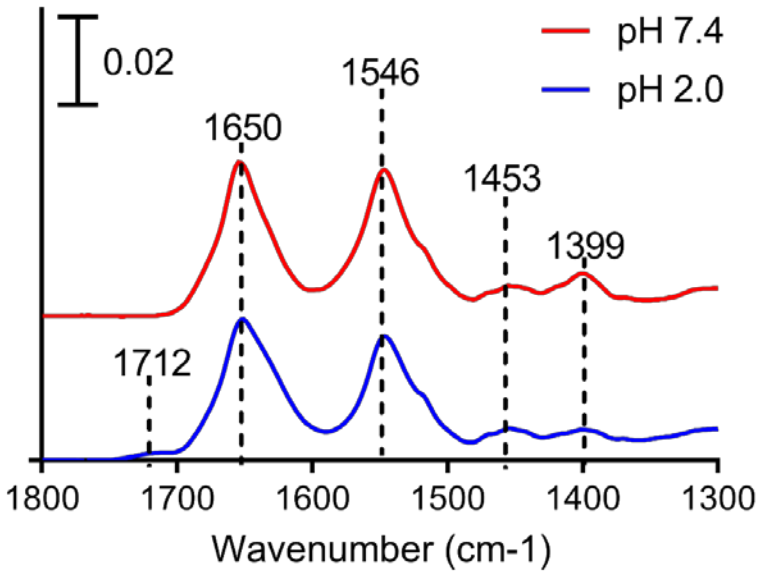

Figure 3-3. Spectra for 10 mg/mL BSA in solution at pH 7.4 and pH 2.0 in the amide regions. Labeled peaks are: the protonated carboxyl group (1712 cm^{-1}), the amide I peak (1650 cm^{-1}), the amide II peak (1546 cm^{-1}), and the amide II peaks (1453 and 1399 cm^{-1}).

In the presence of a nanoparticle substrate, the absorbance intensity of BSA is enhanced by the intermolecular interactions between protein and nanoparticles (Figure 3-4). There were also small shifts in frequency due to changes in the interaction with the surface and other co-adsorbed BSA molecules. In particular, hydrogen bonds cause peak shifts to lower wavenumbers [122], and increased beta units in the protein secondary structure cause peak shifts to higher wavenumbers

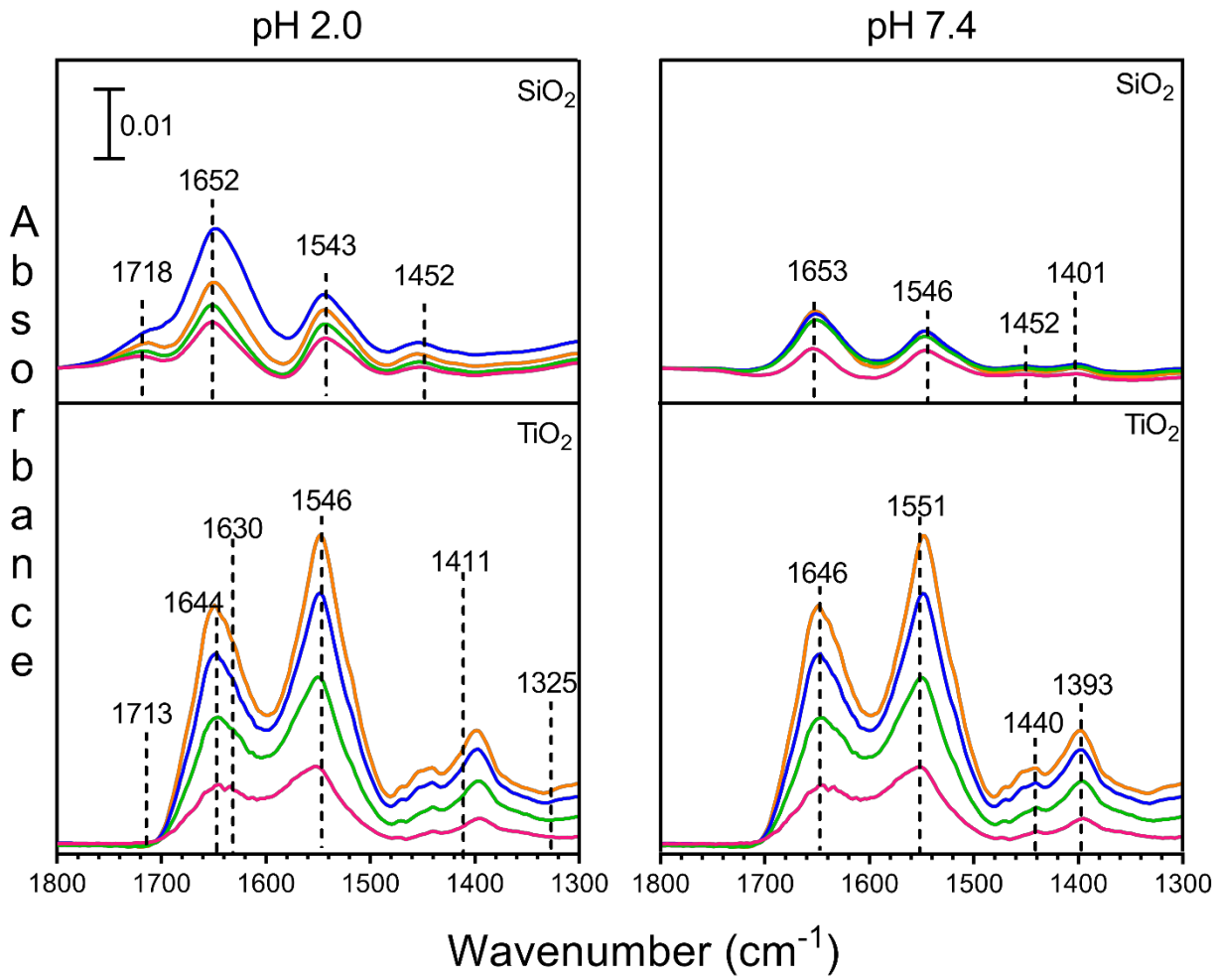

Figure 3-4. Absorbance of 1 mg/mL BSA onto silica and titanium dioxide nanoparticle surfaces as a function of time at two different pH values. Spectra are given for four time points: 10 minutes (pink), 30 minutes (green), 60 minutes (blue), and 90 minutes (orange).

[123]. Figure 3-4 displays the ATR spectra for BSA adsorption to nanoparticle surfaces over time at pH 7.4 (right hand side) and pH 2.0 (left hand side).

Initially, absorbance signal for adsorbed BSA and qualitatively BSA adsorption was greater on the TiO_2 surface than the silica surface. At both pH values, the spectra for BSA adsorbed onto silica did not undergo large peak shifts in either direction. However, at pH 2.0 on the TiO_2 surface, the IR peaks underwent broadening, increased intensity, and frequency shifts in the amide regions. These changes are indicative of protein unfolding and/or denaturing on the nanoparticle surface [67, 124]. A new peak arose at 1411 cm^{-1} at pH 2.0 on the TiO_2 surface as well as a result

of the symmetric stretching mode of COO^- in BSA attached to the highly hydroxylated TiO_2 surface at acidic pH [61, 125, 126]. Additionally, the amide I peak separates into two peaks due to the asymmetric stretching mode of NH_3^+ in highly charged amino acids of BSA [61, 126].

Qualitative information about the protein secondary structure may be obtained from the amide II/amide I peak ratio [68]. The relative intensities of these two peaks, the amide I/II ratio, changes when protein adsorbs to a nanoparticle surface. Along with the knowledge of amide I peak shifts in IR spectra, the amide I/II ratio implies BSA conformational changes at a single pH differed due to the nanoparticle substrate. More specifically, the conformational change of BSA arose from changes in the beta sheet and beta turn structures, consistent with the literature [123].

3.5 Secondary structure analysis of free and adsorbed BSA

To further determine changes in protein structure upon adsorption, spectra for BSA in the solution phase, adsorbed on TiO_2 nanoparticles, and adsorbed on silica nanoparticles at pH 7.4 and pH 2.0 were curve fit using five component bands representative of the protein secondary structure [67, 68, 112]. The amide I bands were curve fit for BSA in solution and BSA adsorbed to either nanoparticle surface and then normalized to have a linear baseline and a peak height of exactly 1.0 absolute absorbance units (Figure 3-5). These normalized spectra can be directly compared for percent secondary structure content of BSA, which are presented in Table 3-1. The literature values for the secondary structure elements of BSA vary over a range of approximately 10%, however, the native alpha helix content of BSA in standard conditions is about 60-65% of the total secondary structure [51, 112, 127-131]. Therefore, for these studies, changes in secondary structure greater than 10% from the solution phase to the adsorbed phase at the same pH were considered significant.

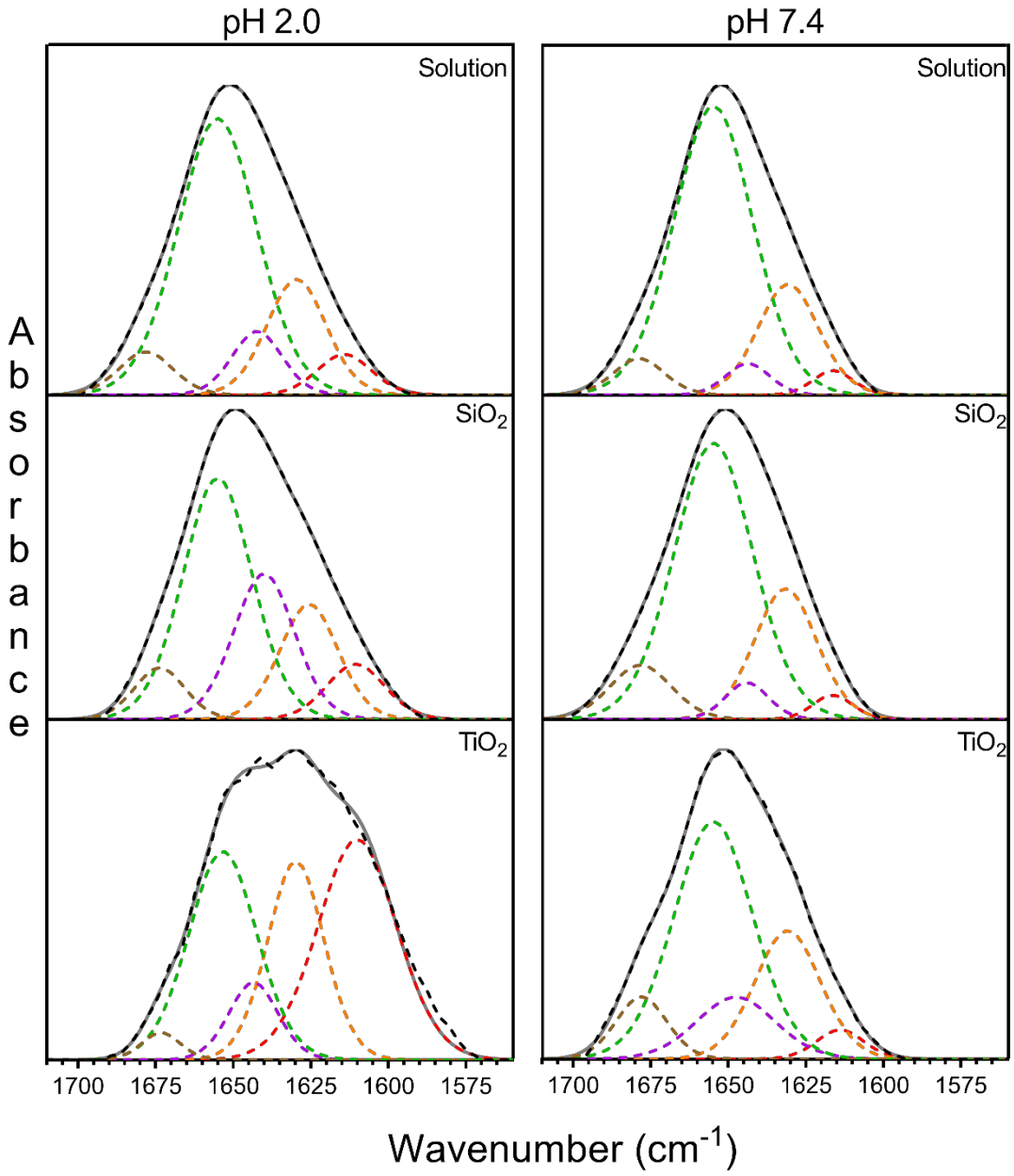

Figure 3-5. Amide I band curve fitting for protein secondary structure of BSA free in solution and adsorbed to either nanoparticle surface. The peaks were fit with five components: beta sheet or beta turn (brown, dotted), alpha helix (green, dotted), random chains (purple, dotted), extended chains or beta sheets (orange, dotted), and side chain moieties (red, dotted). Additional lines shown for baseline (black, solid) and original spectra (black, dotted), as well as the overall fit (gray, solid) for the solution phase (left) and the adsorbed phase (right).

Comparing solely the solution phase BSA at pH 7.4 and pH 2.0 reveals that BSA has decreased alpha helix content at pH 2.0, which is consistent with the literature [132, 133]. This is expected as BSA assumes the extended conformation at lowered pH and therefore loses the tight

secondary structures that form the native heart-shaped molecule [105, 106]. Likewise, adsorbed BSA at pH 2.0 had lower alpha helix content than adsorbed BSA at pH 7.4 on either nanoparticle surface. However, adsorption to the TiO_2 surface caused a much higher decrease in alpha helix content, approximately double that compared to the silica surface at pH 2.0. At the physiological pH, adsorption to the nanoparticle surfaces caused an increase in random chain content and a decrease in alpha helix content on both surfaces. In addition to the loss of alpha helical structure upon adsorption to the silica nanoparticle surface, BSA also loses some of the extended chain and beta sheet structures.

Table 3-1. The secondary structure content (%) in BSA determined via curve fitting for BSA in solution and after adsorption on to the nanoparticle surfaces; silica and TiO_2. (Reproduced with permission from Elsevier, B. E. Givens, Z. Xu, J. Fiegel, and V. H. Grassian, J Colloid and Interface Sci, 493, 2017, 334-341, Table 3.)

pH	Secondary structure	Solution phase BSA	Adsorbed BSA on silica (Δ from solution)[a]	Adsorbed BSA on TiO_2 (Δ from solution)[a]
7.4	β-sheets/turns	5	9 (+4)	9 (+4)
	α-helices	68	59 (-9)	51 (-17)
	Random chains	4	15 (+11)	13 (+9)
	Extended chains/β-sheets	20	12 (-8)	23 (+3)
	Side chain moieties	3	5 (+2)	4 (+1)
2.0	β-sheets/turns	6	5 (-1)	2 (-4)
	α-helices	60	48 (-12)	30 (-30)
	Random chains	9	15 (+6)	8 (-1)
	Extended chains/β-sheets	19	25 (+16)	24 (+15)
	Side chain moieties	6	7 (+1)	36 (+30)

[a] – difference between adsorbed and solution phase structure content

According to the literature, loss of alpha helix structure is balanced by an increase in beta structures, due to higher relative stability [68]. However, the greatest loss of alpha helix structure was observed when BSA adsorbed to the TiO_2 nanoparticle surface, and the major increase was in the side chain moieties, which are due to the unique R groups for each amino acid, rather than the

repeated units in amino acids [67, 68]. This suggests that the side chains became exposed upon protein adsorption to the nanoparticle surface and is therefore indicative of protein denaturation. On the silica surface, the increase was in the beta structures and there was relatively no change in the side chain moieties at pH 2.0. Thus, protein denaturation is more a surface effect than a pH effect.

These data on the changes in secondary structure of BSA are consistent with the frequency shifts of the adsorption bands in the ATR-FTIR spectra (Figure 3-4). BSA adsorbed to the silica nanoparticle surface had very small peak shifts in location, and these peaks maintained their normal shape. However, on the TiO_2 nanoparticle surface, peak shifts to different wavenumbers were greater, and the peaks became broader and less defined. These observations can be attributed to the hydrogen bonds with surface hydroxyl groups [122, 125].

Although both metal oxide nanoparticles have hydroxyl groups present on their surfaces, TiO_2 nanoparticles have a higher surface density of hydroxyl groups than silica nanoparticles [76]. Furthermore, as the number of surface hydroxyl groups increases, so does the affinity for the protein to adsorb to the nanoparticle surface [76, 125, 134]. Therefore, on a hydrated nanoparticle surface, as was the case in these ATR-FTIR studies, BSA has a greater affinity and binding strength to the TiO_2 surface than the silica surface. In addition to hydrogen bonds, which can be confirmed from peak shifts in the IR region, electrostatic interactions between the protein and nanoparticle have been reported to influence protein adsorption [135]. Specifically, the deprotonated carboxylic acid group and the protonated amine groups in the amino acid backbone interact with nanoparticle surfaces in a charge-dependent manner [135].

This leads to a discussion of whether BSA binds to these nanoparticle surfaces as part of their hard or soft protein corona. The soft corona contains proteins that adsorb quickly, but

reversibly to the nanoparticle surface. The hard corona contains proteins that adsorb slowly, but irreversibly to the nanoparticle surface [43, 136]. Additionally, proteins that are in a hard corona state tend to undergo greater conformational changes on the nanoparticle surface than soft corona proteins [69, 136]. Given the protein secondary structure information and the changes in peak location and peak shape in ATR-FTIR, it is probable that BSA is part of a hard corona in the TiO_2 surface, but the soft corona on the silica nanoparticle surface.

Previously, ATR-FTIR spectra have been used to quantify the adsorption of proteins and amino acids to the nanoparticle surfaces [22, 61, 62, 137]. However, this technique requires saturation of the protein on the nanoparticle surface, which could not be achieved for either silica or TiO_2 nanoparticles. Therefore, the thermogravimetric analysis technique was used to quantify protein adsorption to the nanoparticle surface [51].

3.6 Quantification of protein adsorption onto the nanoparticle surfaces

Quantitative protein adsorption was obtained through thermal desorption of protein from the nanoparticle surfaces. Particles were incubated with protein for 24 hours at 4ºC, at which point an equilibrium was assumed for BSA on the nanoparticle surface, although this does not account for multi-layer protein adsorption. The literature values for BSA adsorption onto similar silica or TiO_2 nanoparticles are usually on the order of 10^{11} molecules BSA/cm^2 nanoparticle surface [82, 124, 138, 139]. In these studies, surface coverage was also on the order of 10^{11} molecules (Table 3-2), with the adsorption to the TiO_2 surface at pH 7.4 being the greatest and on the order of 10^{12}.

Table 3-2. Surface coverage for BSA on nanoparticle surfaces at two pH values

	Surface coverage (molecules/cm^2)	
	pH 7.4	**pH 2.0**
BSA on TiO_2	$1.7 \pm 0.3 \times 10^{12}$	$4.6 \pm 0.7 \times 10^{11}$
BSA on Silica	$1.9 \pm 0.3 \times 10^{11}$	$1.5 \pm 0.2 \times 10^{11}$

The differences observed for TiO_2 and silica nanoparticles at the same pH, and at different pH values may be due to the availability of binding sites, specifically for hydrogen bonds between protein and nanoparticle surface [50, 140]. Silica nanoparticles have about half the hydroxyl density as TiO_2 nanoparticles [76], which corresponds with lower quantities of protein adsorption, as observed. For fumed silica, this difference may be even greater as the presence of carbon due to combustion further decreases surface hydroxylation [76]. Furthermore, the terminal hydroxyl groups on the nanoparticle surfaces are affected by the solution pH, with lower numbers of these groups at lower pH where they become protonated [50].

The literature cites both the isoelectric point of the substrate and the protein as important values that mediate adsorption [50, 123, 138, 141]. With these data, it is clear that pH plays a role in adsorption at other pH values as well. An additional consideration not fully investigated through these studies is the number of surface sites occupied by BSA in the normal versus the extended conformation. It is expected that the extended conformation would occupy more surface sites than the normal conformation, and thus could be an additional factor in decreased adsorption on each nanoparticle surface compared with the physiological pH [142].

3.7 Conclusion

The data obtained from these experiments provide information on the effects of the nanoparticle substrate on protein corona formation, rather than the effects of proteins and their suspending solutions. The pH values chosen for these studies highlight two important regions of the body: the majority of the body which operates at pH 7.4 and the stomach which operates at pH 2.0 and contributes to the majority of food digestion. As a function of pH, with a consistent model protein, these nanoparticle substrates lead to distinct responses. In particular:

1. Protein conformation changes as a function of pH both in solution and when adsorption onto nanoparticle surface,
2. Protein conformation differs on the metal oxide nanoparticle surfaces compared to that of protein in solution at both pH values,
3. Protein interactions are stronger with the TiO_2 surface than with the silica surface determined from increased surface coverage and changes in protein conformation.

These studies also show that pH can influence protein-nanoparticle interactions, where acidic pH values lead to greater protein denaturation when adsorbed to a nanoparticle surface. However, pH is not necessarily a driving force for protein denaturation, which depends on the strength of interactions with the nanoparticle surface. There is now evidence that the strength of interactions between BSA and metal oxide nanoparticles may be predicted by the surface hydroxyl group density on the nanoparticle surface. A larger amount of surface hydroxyl groups resulted in stronger interactions between the protein and the nanoparticle surface. However, this is not necessarily the only predictor of nanoparticle-protein interactions.

Although these novel studies showed a new phenomenon of nanoparticle-protein interactions, the literature states that electrostatic interactions are a large driving force for such attraction [74, 125, 143]. Thus, further studies investigated the adsorption of BSA dissolved in various ionic salt solutions onto the silica nanoparticle surface.

This chapter was formatted based on the following publication: Givens, B.E., et al, *Bovine serum albumin adsorption on SiO_2 and TiO_2 nanoparticle surfaces at circumneutral and acidic pH: A tale of two nano-bio surface interactions*, Journal of Colloid and Interface Science, 2017. **493**: p. 334-41.

Chapter 4 The effect of solution ions on the protein corona

4.1 Introduction

Protein adsorption onto nanoparticle surfaces was shown to vary as a function of both pH and the nanoparticle substrate in this work. However, there is also evidence that other solution components alter protein adsorption to nanoparticle surfaces [99, 144]. Additionally, different ion solutions have been shown to shift the isoelectric point of BSA and other proteins [107], which then may alter the adsorption of BSA to nanoparticle surfaces. Therefore, we investigated the effect of changing ionic salts on nanoparticle aggregation, zeta potential, and adsorption of BSA to the silica nanoparticle surface.

First, PBS and acetate buffer were used to determine if effects in water at the pH of greatest adsorption, pH 3.7, and the physiological pH, pH 7.4, were maintained in a more complex solution. Then, salt solutions were prepared based on the ionic concentration found in phosphate buffered saline, as a commonly used buffer for biological solutions. The salts chosen for these studies were also influenced by periodic table groups. There has been research showing aggregation of silica nanoparticles is reduced in Group 2 chlorides due to the electrostatic double layer formed on the nanoparticles, compared with Group 1 chlorides [23, 145]. Thus, both a group 1 chloride and a group 2 chloride were used, but concentrations vary based on the largest relevant unit of PBS.

Many of the chosen solutions were previously investigated with other metal oxide nanoparticles, and it was found that phosphate competitively adsorbs with protein to the nanoparticle surface [73]. Unfortunately, the primary ATR-FTIR peak for silica overlaps with the primary phosphate peak [73, 146], therefore ATR-FTIR studies were not conducted for this effect. The studies that were chosen, including DLS, laser Doppler velocimetry, TGA, and the Derjaguin-

Landau-Verwey-Overbeek (DLVO) model, were done so to improve the understanding of the driving forces behind protein corona formation *in vivo*. The use of simple solutions, rather than the true human fluids, are necessary in order to determine the forces acting upon the nanoparticle and protein. However, without advancing to the complex solutions and *in vivo* studies, a complete understanding is not possible.

4.2 Materials and methods

To confirm results that were presented in chapter 2, two buffered solutions at the physiological pH and at the pH of greatest adsorption were prepared. Acetate buffer was prepared with acetic acid and sodium acetate and adjusted to pH 3.7 using 1M HCl and 0.8M NaOH. Phosphate buffered saline (PBS) was prepared using both sodium and potassium salts and adjusted to pH 7.4 with 1M HCl and 0.8M NaOH. To study the effects of ions and ionic strength, additional solutions were prepared using the ion concentration in PBS as a guide: (a) 10 mM sodium chloride, (b) 130 mM sodium chloride, (c) 70 mM calcium chloride, and (d) 12 mM sodium phosphate.

DLVO theory was used to predict which solution would perform best at resisting the natural tendency for aggregation. The net interparticle forces, V_{net}, for the different solution types were found with DLVO theory, explained in Equations 1-4 [102].

$$V_{net} = V_{vdw} + V_{elec} \tag{1}$$

V_{vdw} is the attractive forces (J) of the particles and V_{elec} is the repulsive forces (J) of the particles, given by Equations 2 and 3, respectively.

$$V_{vdw} = \frac{-A_H}{12} \times \left(\frac{y}{x^2 + xy + x} + \frac{y}{x^2 + xy + x + y} + 2 \ln \left(\frac{x^2 + xy + x}{x^2 + xy + x + y} \right) \right) \tag{2}$$

A_H is the Hamaker's constant for silica in water, 4.6 x 10^{-21} J [147]. For silica nanoparticles of constant size, y = 1 and x = d/(2R), where d is the distance between particle surfaces (m) and R is the particle radius (m).

$$V_{elec} = 2\pi\varepsilon_r\varepsilon_0\Psi_0^2 R k_B T \times \ln(1 + \exp(-\kappa d)) \quad (3)$$

ε_r is the relative dielectric constant of the liquid (80.1 for water) and ε_0 is the permittivity of a vacuum, 8.85 x 10^{-12} C^2/J-m. The measured zeta potential, in volts, was used for the value of Ψ. k_B is Boltzmann constant, 1.38 x 10^{-23} J/K. T is temperature, given in units of Kelvin. κ was calculated from e (elementary charge, 1.6 x 10^{-19} C), N_A (Avogadro constant, 6.02 x 10^{23} mol^{-1}), and I (ionic strength of the solution in mol/m^3):

$$\kappa = \left[\frac{e^2 N_A(2I)}{\varepsilon_r\varepsilon_0 k_B T}\right]^{0.5} \quad (4)$$

The extended DLVO model has been developed to include forces due to interparticle interactions between adsorbed surface ligands, rather than the nanoparticle surfaces [23]. The osmotic force depends upon the molecular volume of the solvent (v_1), volume fraction of polymer within the coating layer (Φ_p), the Flory-Huggins interaction parameter (χ), the particle radius (R), the polymer layer thickness (w), and the separation distance between particles (d), and varies for three different regions (Equations 5-7).

$$V_{osm} = 0 \; for \; (2w \le d) \quad (5)$$

$$V_{osm} = \frac{4\pi R k_B T}{v_1}\Phi_p^2\left(\frac{1}{2} - \chi\right)\left(w - \frac{d}{2}\right)^2 \qquad w \le d < 2w \quad (6)$$

$$V_{osm} = \frac{4\pi R k_B T}{v_1}\phi_p^2\left(\frac{1}{2} - \chi\right)w^2\left(\frac{d}{2w} - \frac{1}{4} - \ln\left(\frac{d}{w}\right)\right) \qquad for \; (d < w) \quad (7)$$

The elastic repulsive energy is due to entropy loss that occurs upon compression of the coating layer and is considered to give a significant contribution when the distance between particles is less than the particle diameter [102, 148, 149].

$$V_{elas} = 0 \qquad for\ (w \leq d) \tag{8}$$

$$V_{elas} = \frac{2\pi R k_B T}{v_1}\phi_p d^2 \rho_p \left(\frac{d}{w}\ln\left[\frac{d}{w}\left(\frac{3-\frac{d}{w}}{2}\right)^2\right]\right) - 6k_B T ln\left(\frac{3-\frac{d}{w}}{2}\right) + 3k_B T\left(1+\frac{d}{w}\right)$$

$$for\ (w > d) \tag{9}$$

Thus, including the extended DLVO model, the total interaction energy becomes

$$V_{net} = V_{vdw} + V_{elec} + V_{osm} + V_{elas} \tag{10}.$$

This model is advantageous to this study as we confirm BSA is adsorbed to the nanoparticle surface.

4.3 Aggregate diameter and zeta potential in aqueous media

The hydrodynamic diameter (Figure 4-1) and zeta potential (Figure 4-2) of particles in solution can be compared across various concentrations of ions and between bare particles and coated particles. The two-way ANOVA analysis comparing the uncoated silica to the coated silica revealed statistical significance for differences in hydrodynamic diameter in all solutions to a p value less than 0.0001 except sodium phosphate solution. The changes in zeta potential in each solution with the addition of BSA are significant to $p < 0.0001$ for both sodium chloride solutions, and acetate buffer. Therefore, BSA does not alter aggregation or zeta potential in sodium phosphate solution. Furthermore, the lowest observed hydrodynamic diameter and zeta potential values were in the presence of BSA was in sodium phosphate solution.

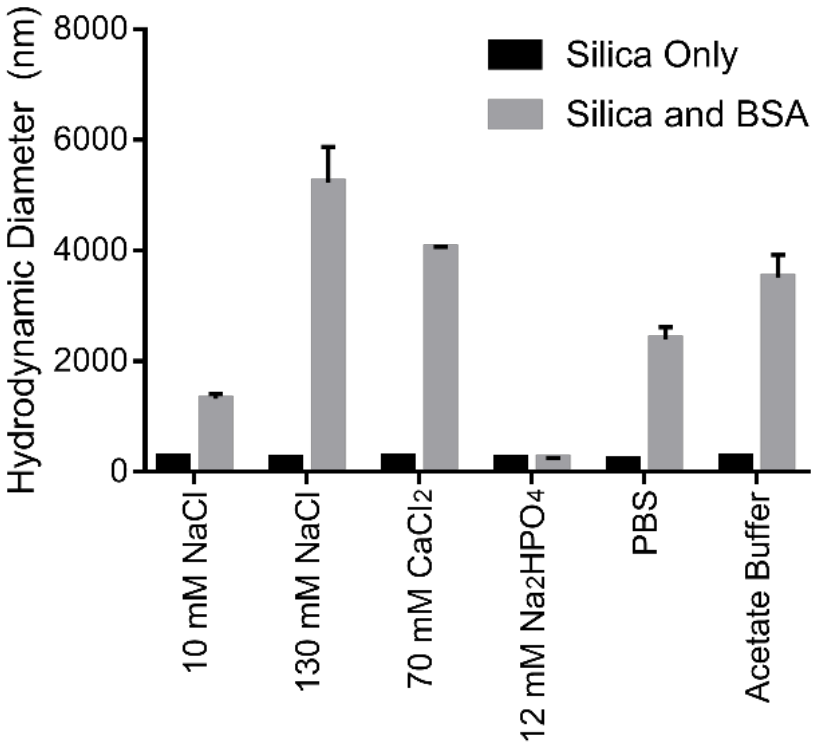

Figure 4-1. Hydrodynamic diameter of silica nanoparticle in the presence and absence of BSA as a function of solution ions

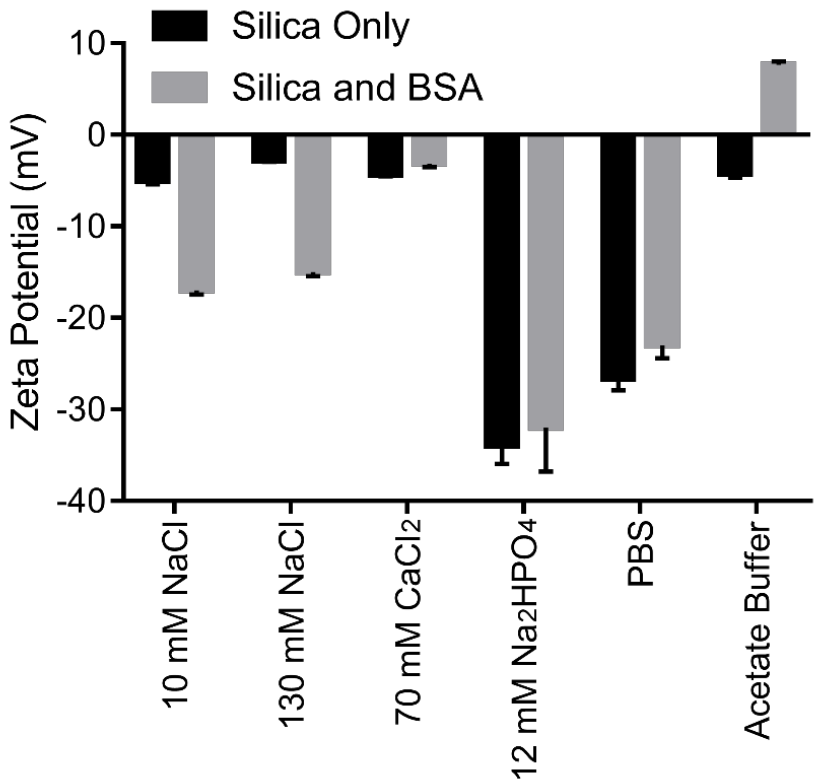

Figure 4-2. Zeta potential of silica nanoparticles with and without BSA coatings as a function of solution ions

The differences between hydrodynamic diameter and zeta potential for either silica or silica coated with BSA in difference solutions are more complicated. In the presence of BSA, by two-way ANOVA, there is a significant difference between zeta potential for all combinations of solution comparision, except 10 mM NaCl and 130 mM NaCl. This suggests that the concentration of NaCl in solution does not affect the zeta potential of the protein, and could warrant further investigation. Additionally, both in the presence and absence of BSA, all solutions exhibited significant differences from PBS, which was the primary solution from which all others were chosen.

A comparison between water at the same pH of the buffered solutions, pH 7.4 and pH 3.7, was conducted to determine if the presence of ions in solution has an effect apart from the pH effect on the hydrodynamic diameter (Figure 4-3) and the zeta potential (Figure 4-4). In the

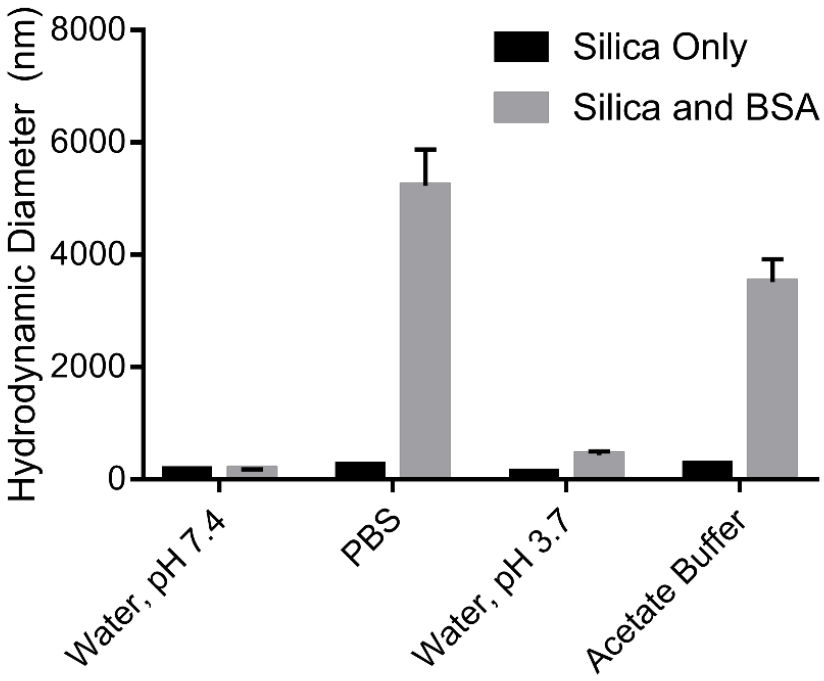

Figure 4-3. Hydrodynamic diameter of silica nanoparticles in the presence and absence of BSA in pH-adjusted water and buffered solutions

presence of BSA, aggregation in the buffered solutions is at least 10-times greater than in pH-adjusted water. The zeta potential measurements are similar for PBS as with water, and in the presence of BSA the error is too large to discern any differences. In acetate buffer, silica nanoparticles exhibit almost exactly the same zeta potential as in pH-adjusted water, and both have very low error associated with them. This suggests that any effects of pH and/or ions occurs on the protein rather than the nanoparticle.

From this information, it is unclear whether ions further affect protein adsorption to the nanoparticle surface. In one school of thought, if the ions adsorb to the nanoparticle surface, they occupy available surface sites onto which the protein would otherwise bind. Similarly, the presence

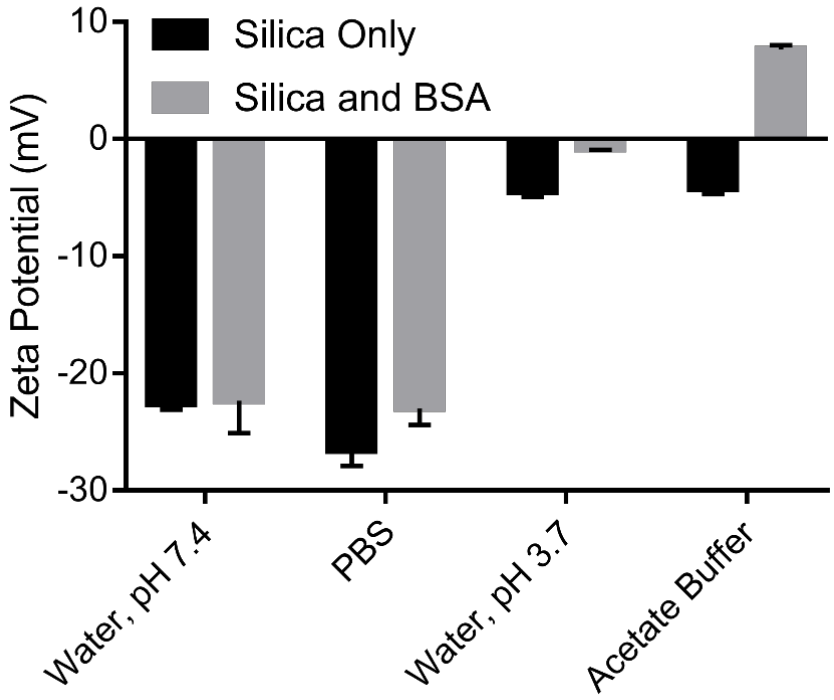

Figure 4-4. Zeta potential measurements for silica and silica coated with BSA in pH-adjusted water and buffered solutions

of ions and protein affects the tendency towards aggregation, thus other nanoparticles may also occupy otherwise available surface sites.

4.4 Quantifying protein adsorption to the nanoparticle surface in different mediums

Comparing pH-adjusted water to buffered solutions at the same pH values revealed that greater protein adsorption occurred in the presence of ions (Figure 4-5). This suggests that the affinity for the protein towards the nanoparticle surface is in fact altered in ion-containing solutions. An important consideration dominating these interactions is that ions are charged particles; therefore, any adsorption of an ion to the nanoparticle surface will alter the surface charge of the nanoparticle. Since it is known that both hydrophilicity and net charge of the nanoparticle

surface influence protein adsorption [67, 68, 70, 71], this could explain differences between salt solutions and water.

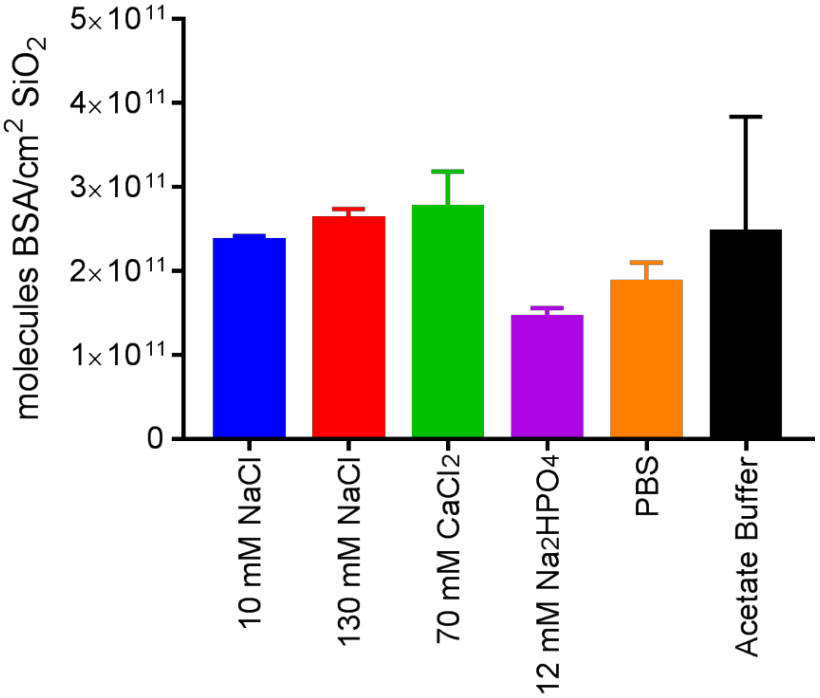

Figure 4-5. TGA analysis for the surface coverage of BSA on silica nanoparticles in molecules protein per nanoparticle surface area

4.5 Theoretical model of inter-particle interactions

The DLVO theory was used to model potential interparticle interactions in aqueous solutions (Figure 4-6). This theory has been used by others to model the interaction energy in colloidal suspensions, particularly biomolecule-nanoparticle interactions [20, 74, 102]. As nanoparticle size affects biological interactions, and these particles are present in fused aggregates, models using both the primary particle size (a, b) and the aggregate diameter were investigated (c, d). The energy barrier, or the height of the interaction energy, is the primary factor determining colloidal stability. In order for particles to remain separate, the interaction energy must be higher than the energy of Brownian motion, around 1.5kT [102]. In these studies, sodium phosphate solution always had a higher interaction energy than that of Brownian motion, and therefore

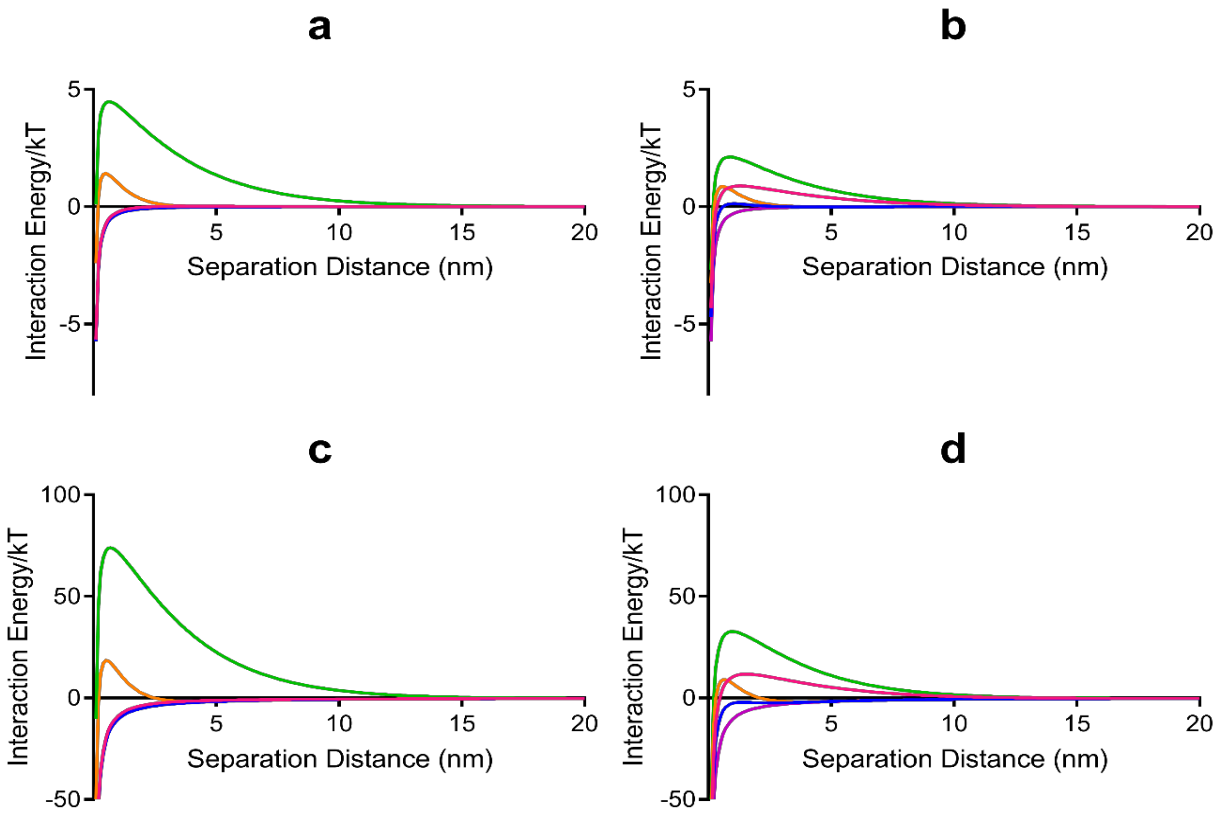

Figure 4-6. DLVO model for interactions between nanoparticles of size 14 nm without a protein corona (a) and with a protein corona (b), and particles of 250 nm in diameter without a protein corona (c) and with a protein corona (d). Data are presented for 10 mM NaCl (pink), 130 mM NaCl (blue), 70 mM $CaCl_2$ (purple), 12 mM Na_2HPO_4 (green), and PBS (orange).

particle aggregation was reduced. This was confirmed with results from DLS when the addition of BSA to the nanoparticle suspension did not result in further aggregation. This is also true regardless of which primary nanoparticle size was used for calculations.

The larger assumed nanoparticle diameter, 250 nm, resulted in greater energy barriers than the smaller particles. This is logical as nanoparticles are less stable in solution than their bulk counterparts [150]. Additionally, the presence of BSA decreases repulsive interactions as compared with silica alone in solution. This agrees well with the hydrodynamic diameter measurements, which show consistent diameters for silica in all solutions, which are also consistent with the measured aggregate diameter in TEM. However, in the presence of BSA,

aggregation increases dramatically with these salt solutions and therefore attractive interactions must also be increasing.

Furthermore, in the presence of BSA, the range of values for the energy barriers narrows. That is, there is greater variability in the stability of silica nanoparticles in the absence of BSA than in the presence of the protein. Even so, there are some solutions, which consistently show interactions will always be attractive, that is, the energy barrier is always negative. This occurs for calcium chloride and 130 mM sodium chloride, suggesting that aggregation can never be eliminated in these solutions. In the absence of BSA, this is also true of 10 mM NaCl, however, with the addition of BSA, this energy barrier exceeds that for PBS. The energy barrier for particles in PBS does not change upon the introduction of BSA.

The extended DLVO model is advantageous for systems in which a new layer of surface ligands is generated on the nanoparticle surface [148]. This model depends on additional parameters, and takes into account additional interactive forces which may be imparted on the system by the surface ligands; in particular, this model accounts for the additional steric interactions [102]. The downfall to this model in protein-nanoparticle systems, is choosing the correct parameters in the extended model to correctly model the system. In particular, the volume fraction of polymer within the coating layer (Φ_p), the Flory-Huggins interaction parameter (χ), and the polymer layer thickness (w) presented issues with this system.

The Flory-Huggins interaction parameter is a thermodynamic parameter which accounts for interactions between a polymer molecule and its nearest neighbors [151]. According to the Flory-Huggins model, the boundary between a good solvent and a poor solvent occurs at $\chi = 0.5$

[151, 152]. In the literature, this parameter is generally assumed to be 0.45 [102, 149], slightly within the range of a good solvent [151, 152].

The volume fraction and the polymer layer thickness both must be determined experimentally, which can be done using particle sizing techniques such as TEM [102]. TEM was not completed for these coated particles, and assessing the protein coating on an aggregate of particles is challenging. Determining whether to use the fraction of coating on the individual particles or the aggregate is difficult, particularly when trying to consider the outermost layer, or all of the pores between individual nanoparticles. Therefore, it was determined that although the extended DLVO model is advantageous for describing a nanoparticle with a protein corona, these nanoparticles are not well suited for this analysis.

4.6 Conclusion

A model system for determining protein-nanoparticle interactions is useful in determining the small-scale driving forces for these interactions. In this chapter, the model system was silica nanoparticles, bovine serum albumin protein, and various salt solutions. Previous literature has shown that certain ions, such as phosphate, may competitively adsorb to a metal oxide nanoparticle surface [73]. Other literature has shown that the molecular weight and/or the periodic group affect aggregation [23, 145]. These studies were designed to highlight these differences and compare them.

Results indicated that sodium phosphate provides the greatest repulsion of silica nanoparticles in the presence of BSA, and no additional aggregation occurs with the addition of BSA, unlike the other solutions. We also found that protein adsorption onto the silica nanoparticle surface was greater in the presence of ions than in pure water at the same pH value, which indicates that the ions generate a more favorable surface for protein binding. The implications of increased

affinity for proteins to adsorb to the nanoparticle surface as well as aggregation are significant for the field of bionanotechnology. As the true biological fluid these nanoparticles will be dispersed in has more ions than pure water, these differences are critical to understand when developing drugs, sensors, or other biological applications for silica nanoparticles.

This chapter was formatted based on the following publication: Givens, B.E., et al, *The Effect of Solution Properties on Protein Corona Formation*, 2017. *In preparation*.

Chapter 5 Toxicity in vitro of nanoparticles with and without a protein corona in A549 cells

5.1 Introduction

The potential for nanoparticles to induce cytotoxicity in target organs is of great concern for occupational health, environmental health, and drug delivery [38]. Thus, assessing the toxicity of nanoparticles, which have been approved for pharmaceutical and food use in human cells is a necessary step towards assessing their safety and efficacy in these applications.

A549 cells are a commonly used toxicity model, and are an excellent starting point for studies because they have been so widely used. Most of these toxicity tests include a dose-dependent response, in which a wide range of nanoparticle doses are exposed to cells in vitro and the cytotoxicity is compared across this dose range [29, 153]. In particular, one study showed that serum-free culture media has a greater dose-dependent effect than complete medium, which showed no dose-dependence [99]. Dose-dependence is an important concept in the toxicity realm because the minimum effective dose and the minimum toxic dose are both of critical importance with safe design [19, 154, 155].

Metal oxide nanoparticles are typically used in toxicity studies because they can readily oxidize to different states [156], and/or they can leach ions into the biological environment inducing toxicity [97]. There is evidence in the literature that silica nanoparticles can cause toxic responses in cell lines, despite the common belief that amorphous silica is nontoxic [29, 66, 72, 97, 157-162]. In particular, the presence of proteins on the nanoparticle surface is shown to enhance adverse responses by the cells [163, 164]. However, certain protein coronas may mitigate the toxic effects of silica [165].

For the studies presented herein, we aimed to investigate both the dose-dependent response of A549 human adenocarcinoma lung cells to silica nanoparticles with and without a bovine serum albumin protein corona. We hypothesized that higher doses of nanoparticles would lead to greater cytotoxicity regardless of the presence of serum, and that the cytotoxicity for the same dose would be greater in complete serum-free conditions compared with nanoparticles coated with a BSA corona.

5.2 Materials and methods

A549 adenocarcinoma lung cells were gifted from Peter Thorne. Cells were maintained in T75 flasks and passaged every 4-6 days. Cell culture media was prepared using Roswell Park Memorial Institute (RPMI, Gibco) media supplemented with 10% fetal bovine serum (FBS, Atlanta Biologicals) and 1% penicillin/streptomycin (Life Technologies). For nanoparticle exposure experiments passage numbers 25-29 were utilized, and cells were plated in a 96-well plate at 1 x 10^4 cells/well and allowed to grow overnight before nanoparticle exposure. In these experiments, serum-free RPMI was used as the cell culture medium.

Silica nanoparticles were suspended in serum-free RPMI media supplemented with 1% penicillin/streptomycin, and allowed to sit overnight at 4ºC to prevent protein denaturation. For particles with a protein corona, 1 mg/mL of BSA was prepared in serum-free RPMI media to which the silica nanoparticles were added. Stock solutions of 200 µg/mL silica were prepared and diluted in serum-free RPMI to other desired concentrations: 150, 100, 50, 25, and 10 µg/mL. Each dose was repeated in triplicate and added to wells in a volume of 100 µL. 24-hours following exposure, nanoparticle toxicity was assessed.

The release of lactate dehydrogenase (LDH) from the cells into the supernatant was measured using the Pierce LDH cytotoxicity assay kit (Thermo Scientific), following the protocol

for chemical-compound mediated cytotoxicity. Briefly, the supernatant was removed from cells and placed in a new 96-well plate. An equal volume of the reaction mixture was added, and the plate was allowed to incubate protected from light at room temperature for 30 minutes before conducting absorbance measurements at 490 nm and 680 nm. The values used for the provided equation (Equation 11) was the absorbance at 680 nm subtracted from the absorbance at 490 nm. Controls for maximum LDH release and spontaneous LDH release were included.

$$\%\ cytotoxicity = \frac{Treated\ LDH\ activity - Spontaneous\ LDH\ activity}{Maximum\ LDH\ activity - Spontaneous\ LDH\ activity} \quad (11)$$

The same cells used for LDH cytotoxicity were treated with 100 µL serum-free RPMI media and 20 µL of MTS reagent (CellTiter 96® AQueous one solution cell proliferation assay, Promega), and incubated for 4 hours at 37ºC, 5% CO_2. After 4 hours, cells were centrifuged at 500-g for 20 minutes and 70 µL of the supernatant was removed and placed in a new 96-well plate to reduce interference from nanoparticles and serum albumin. Absorbance was measured at 490-nm. The cell viability as a percent of the control was calculated by taking the average absorbance for the control groups and dividing each measurement by that average.

The aggregate diameter and zeta potential of the nanoparticles dosed to the cells were measuring using a Malvern ZetaSizer (Nano ZS). These measurements were made from the same solutions that were used for cell exposure, and measurements were taken approximately 24 hours after preparation. Measurements were conducted in triplicate.

5.3 Aggregate diameter and zeta potential of dosed particles

The aggregation and zeta potential were of interest in these studies as nanoparticle size can influence uptake into cells, tissues, and organs [93, 166, 167]. Additionally, the influence of the presence of BSA in cell culture medium was expected to differ from other studies with pH and

solution components. However, these studies were not a primary focus for this work and therefore, only select doses of nanoparticles were investigated (Figure 5-1). Zeta potentials were approximately -11 mV for all conditions, and individual values have not been reported here. Aggregation beyond that which is expected of the native particles did not occur for all conditions, nor did it follow a clear nanoparticle dose-dependent trend. No aggregation was noted for 10 or 50 µg/mL silica in RPMI, and very little aggregation was noted for 50 µg/mL silica and 1 mg/mL BSA in RPMI. However, at 10 µg/mL silica with 1 mg/mL BSA, the average hydrodynamic diameter was very close to 400-nm which could indicate the formation of dimers, although this cannot be confirmed without further analysis. Significant aggregation, over 1 µm, was observed for 200 µg/mL silica with and without 1 mg/mL BSA in RPMI, and 100 µg/mL silica in RPMI. These results suggest that the presence of serum is not the only component of cell culture media, which leads to aggregation for these silica nanoparticles [54, 55].

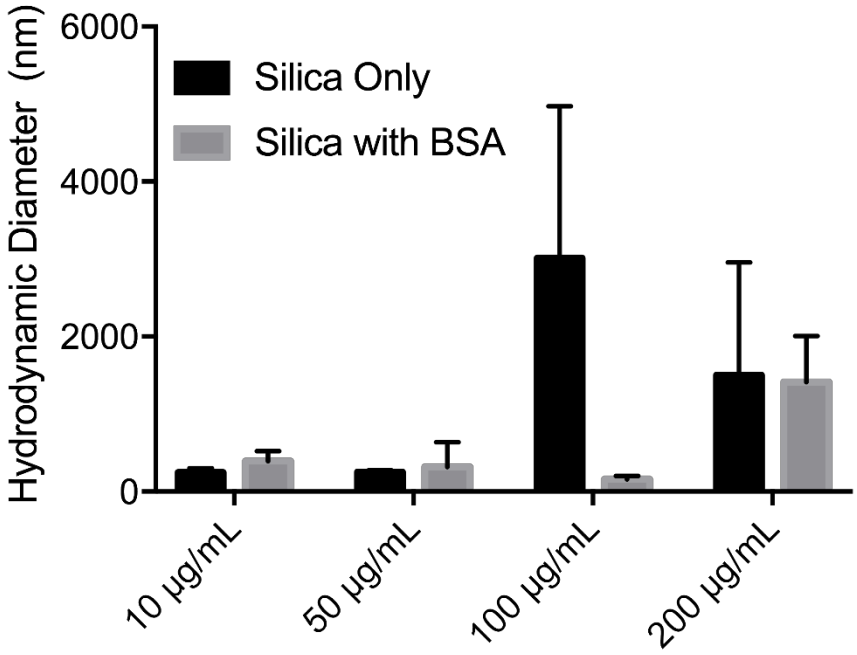

Figure 5-1 Hydrodynamic diameter average ± standard deviation for silica in the presence and absence of BSA in serum-free RPMI

5.4 Cell viability

Two assays were used to assess nanoparticle toxicity on A549 cells, the LDH leakage assay and the MTS metabolic activity assay. The percent cytotoxicity elicited in the cells can be calculated from the measured absorbance in each of these colorimetric assays. The LDH leakage assay (Figure 5-2) showed negative cytotoxicity for both control types, indicating that the lysed cells had less absorbance than the control group. This may be evidence towards interference of nanoparticles and/or residual BSA in solution with the reagent. For other treatment groups, the error displayed within each condition renders drawing conclusions on a dose-dependent or BSA-dependent response difficult. The average value at each condition suggests there may be a dose-dependent response where higher doses of nanoparticles lead to greater cytotoxicity.

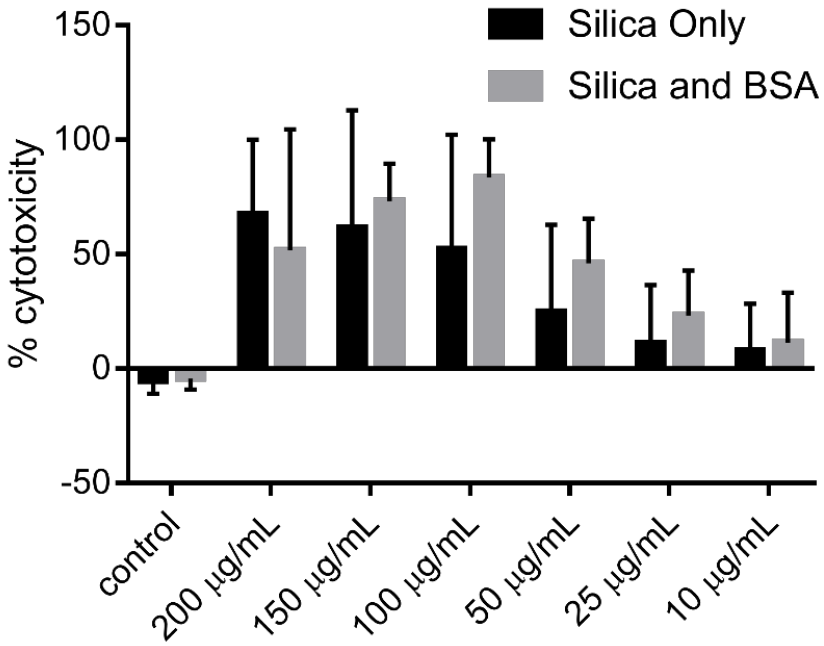

Figure 5-2. LDH leakage assay cytotoxicity towards cells in the presence and absence of BSA. Data are presented as the mean with standard deviation. Control with BSA does not include silica nanoparticles

The MTS assay was also used to assess the metabolic activity in the cells (Figure 5-3). Again, the standard deviation for these measurements is too great to determine whether there is a dose-dependent or BSA-dependent response. However, using the mean values once again suggest there is a dose-dependent response with higher doses leader to greater toxicity. The least variability for this assay was observed in the 150 and 100 µg/mL silica with 1 mg/mL BSA groups. Each of these conditions exhibited a low amount of cell viability with small standard deviations. This

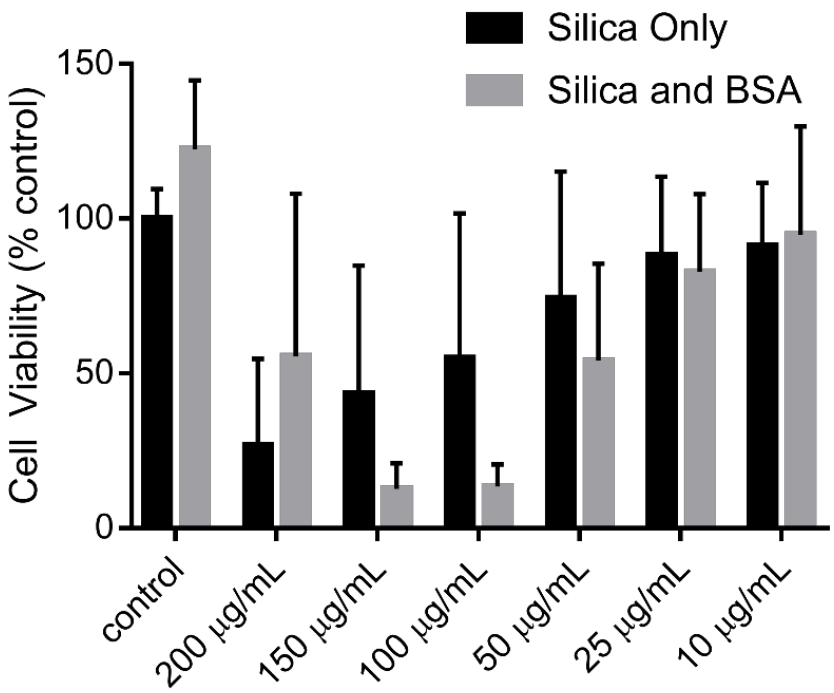

Figure 5-3. MTS metabolic activity in cells as a percent of the control activity in the presence and absence of BSA. Data presented for mean with standard deviation. Control with BSA does not include silica nanoparticles.

contradicts the hypothesis that the presence of serum from BSA aids in cell proliferation in serum-free RPMI.

The relative degree of cytotoxicity is consistent between the two assays; therefore, a greater number of replicates or improved standardization of dosing may be required to obtain accurate data. Although the 150 and 100 µg/mL protein-coated silica doses show unexplained decreases in

cytotoxicity, which do not follow the general dose- or serum-presence response, they are consistent between both cytotoxicity assays.

Although these assays provided agreeable cytotoxicity data, there is a major pitfall to colorimetric assays. The nanoparticles have the ability to bind with the dyes used in the assays and alter the absolute absorbance, as well as the interference of optically active nanoparticles at the measured absorbance values [168-170]. Particles can be removed from solution via centrifugation before the absorbance measurements, but this does not eliminate interference during incubation periods. Additionally, the raw absorbance values (*not shown*) suggest the absorbance may be affected by changing serum concentrations in the test conditions.

5.5 Conclusion

These studies demonstrated a potential dose-dependent response of A549 human adenocarcinoma lung cells to silica nanoparticle with and without an existing protein corona. Nanoparticles in serum-free RPMI or RPMI with 1 mg/mL BSA were administered to cells in a dose-dependent manner. Although the cell culture media was serum-free and BSA could potentially provide the cells with a nutrient known to aide in cell proliferation and integrity, greater cytotoxic responses were observed in the presence of BSA compared to the bare nanoparticles at two doses.

These studies are not sufficient to determine the mechanism of cytotoxicity, but the assays used provided information on cell integrity. Although proliferation was not directly measured, the high percent cytotoxicity for doses greater than or equal to 100 µg/mL silica from the LDH assay indicate that cells had compromised membrane integrity. The resulting viability from MTS, or the metabolic activity of these same cells, revealed that the magnitude of toxicity in LDH was not predictive for impaired mitochondrial function. Therefore, additional studies on nanoparticle

uptake and other measures of cytotoxicity are necessary to determine the mechanism of action and the severity of toxic responses in this system.

Toxicity testing *in vitro* may differ from tests *in vivo* for several reasons, including the increased complexity of an organism over cells, and retention time in tissues [171]. Thus, there is still significant work to be done in this area in assessing the toxicity of silica nanoparticles for food and pharmaceutics. Furthermore, administration *in vivo* is a critical component in determining toxicity, and these lung epithelial cells only provide information for inhaled drug delivery. Thus, while these studies are informative, they are merely a starting point for further experiments.

Chapter 6 Conclusion and Future Directions

6.1 Conclusion

The presence of nanoparticles in the environment and the potential growth of nanoparticle use in biotechnology generate concerns over the human health impacts of nanoparticle exposure. The field of nanotoxicology to assess these potential impacts is still in its infancy and much work still needs to be done. The physicochemical properties of a nanoparticle impact the protein corona and cellular responses *in vitro*. Thus, it is difficult to determine a universal "rule" for how nanoparticles will behave in the body and much testing still needs to be done. Using the current knowledge in the field, we have investigated a commercial silicon dioxide nanoparticle approved for food and pharmaceutical use in various aqueous environments by pH, including that in the stomach, lung, blood stream, and GI tract. Furthermore, we have investigated behavior of these nanoparticles in various saline solutions to improve understanding of how different regions of the body might respond to nanoparticles. Ultimately, these ideas should be integrated and further expanded upon to complete the picture of human responses to nanoparticles.

The goal of this work was to improve the understanding of the effect the environment has on nanoparticle properties and subsequent cellular responses. Chapter 2 focused on the pH-dependent effects on protein-nanoparticle interactions of BSA and silica. The silica nanoparticles were present as fused aggregates, and did not aggregate further in aqueous solution independent of protein, except near the isoelectric point. The zeta potential of these particles changed as a function of pH, however, at the physiological pH the zeta potential of silica was approximately equal in the presence and absence of BSA. ATR-FTIR was used to monitor the real-time adsorption of BSA to the nanoparticle surface and assess protein conformational change on the nanoparticle surface. The characteristic peaks for proteins in the IR spectrum did not shift for BSA

in solution as a function of pH, nor did they shift as a function of BSA adsorption to the nanoparticle surface. BSA continued to adsorb to the nanoparticle surface as a function of time, evidenced by an increase in absolute absorbance. In some cases, the desorption band has a greater intensity than the final adsorption band, which can be explained by conformational changes on the nanoparticle surface. The conformation of BSA on the silica surface was assessed using curve fitting of the amide I peak. The alpha helix content underwent the greatest amount of change of all the structures, and decreased below the typical range for BSA (60-65%) during adsorption, and increased above that range during desorption. At other pH values, the alpha helix content was fairly constant as a function of time and fell within the expected range. The amount of protein adsorbed to the nanoparticle surface was quantified using TGA, and does not vary significantly as a function of pH, except between pH 2.0 and pH 3.0. The maximum adsorption for protein on the nanoparticle surface was at the protein-nanoparticle isoelectric point of pH 3.7 and closely followed by the isoelectric points of the substrate and the protein, respectively. The adsorption at pH 2.0 was the least, which disagrees with the absolute absorbance in ATR which is least at pH 7.4. This discrepancy highlights the importance of using multiple methods to assess protein-nanoparticle interactions between compounding effects can mask true effects.

To build upon the effects observed as a function of pH with BSA on silica, we compared the effects of BSA adsorbed to silica nanoparticles and titanium dioxide nanoparticles as described in chapter 3. The TiO_2 nanoparticles also formed aggregated, but in smaller clusters than silica nanoparticles. The isoelectric point of both materials was experimentally determined using zeta potential values and found to be pH 6.5 and pH 2.7 for TiO_2 and silica, respectively. These values are expected to generate the greatest amount of protein adsorption, according to the previous studies. However, since neither value was investigated for this study, we expected the protein

adsorption to be greater on silica at low pH and greater on TiO_2 at neutral pH. Surface coverage was greatest for BSA on TiO_2 at pH 7.4, however the lowest surface coverage occurred for BSA on silica at pH 2.0. Thus, isoelectric point alone is not a good indicator of protein adsorption, suggesting that electrostatic interactions are not necessarily the driving force for protein adsorption to nanoparticle surfaces. The secondary structure of BSA changed more on the TiO_2 surface than the silica surface, particularly in a decrease in alpha helix structures. BSA also gained extended chains or beta sheets on both particle surfaces, except for silica at pH 7.4. These changes in protein secondary structure suggest BSA is folding on the nanoparticle surface. At pH 2.0, the side chain structures gain a large percentage of the curve fitting area on the TiO_2 surface, which suggests that the protein is severely denatured and exposing the unique R groups to each amino acid, rather than the repeated structure, which provides both the characteristic IR peaks and arranged protein structure. Therefore, the effects of pH on protein adsorption are more severe for TiO_2 nanoparticles than for silica nanoparticles, which has important implications for two nanoparticles used as food additives.

In addition to pH, the concentration and types of ions in the body differ by location. The effects of different ions in solution was the focus of chapter 4. In the presence of ions and BSA, silica aggregates in aqueous solution, unlike in water as a function of pH when aggregation was only observed at the isoelectric point. This was confirmed using two buffered solutions at the pH values 7.4 and 3.7 to compare with water at the same pH values. Aggregation was much greater in buffered solutions compared with pH-adjusted water, but the zeta potentials were approximately equal. Although aggregation increased in the presence of salts, there was one solution that did not cause aggregation or changes in the zeta potential upon the addition of BSA: sodium phosphate. The DLVO theory was used to model the electrostatic and van der Waals interactions between

neighboring nanoparticles in different aqueous solutions with and without BSA. The DLVO calculations revealed the greatest repulsive interactions occurred for particles suspended in sodium phosphate, consistent with the reduced aggregate diameter observed from DLS. PBS also offered some repulsive interactions, but none as strong as sodium phosphate. Additionally, the strength of repulsive interactions was greater for silica nanoparticles in the absence of BSA than in the presence of BSA. Protein adsorption was quantified using TGA and sodium phosphate solution resulted in the least amount of protein adsorption to the nanoparticle surface. These results suggest that sodium phosphate may be an important solution in reducing protein corona formation, nanoparticle aggregation, while maintaining the zeta potential.

The *in vitro* toxicity of silica nanoparticles with and without a protein corona was investigated for chapter 5. The aggregate diameter of nanoparticles in cell culture media as a function of nanoparticle aggregation was measured, and at low concentrations of nanoparticles in culture media there is no additional aggregation, however, at higher concentrations aggregation increases to the micrometer range in the absence of BSA. After nanoparticle exposure, the cell viability was assessed by membrane integrity and metabolic activity. The error associated with these studies was too great to determine whether or not a dose-dependent response existed, which is due to deviation within a single study and repeated trials. In general, it seems that lower concentrations of silica nanoparticles induce less toxicity than higher concentrations.

6.2 Recommendations and future directions

Many of the presented studies have room for growth. The nanoparticle-protein interactions in water were determined to be substrate-dependent as shown in chapter 3. Therefore, these types of studies must be conducted for each nanoparticle and applications, particularly in the nanobiotechnology industry. Additionally, the effects of aggregation differed in water, buffered

solutions, salines, and cell culture media, therefore the dispersant for these nanoparticles is of critical importance. In order to simplify the system and hone in on certain effects, many of these studies were done in water, and no studies were completed in human biological fluids such as whole blood, plasma, or lung fluids. These complex fluids contain a variety of proteins and ions, which will affect the formation and composition of the protein corona. Therefore, once the basic information has been obtained, these fluids are necessary in truly understanding the goings on of nanoparticles in the human body. Furthermore, as mentioned with the cell models, these fluids are in constant motion, and therefore studies which mimic the dynamics of these fluids are also important.

The primary, and ultimate, concern for nanoparticles leached into the environment and/or used for biomedical applications, is how they interact with the human body. Human evidence can only be studied epidemiologically due to ethical and moral reasons, therefore, model systems for the human body are necessary to determine the potential harmful effects of nanoparticles. For this work, an *in vitro* model for the lung was chosen based on its prevalence in the literature, A549 adenocarcinoma human epithelial lung cells from the alveolar region. However, this model has significant disadvantages: (a) cancerous cells cannot accurately model healthy systems, (b) a single-cell model does not accurately represent the complex human environment, and (c) the static lung cell system does not accurately model the mechanical properties in the lung. Therefore, studies with other lung cell lines, co-culture models of the lung, and dynamic models of the lung are all important modifications to this work for future studies. Another important consideration with this model is the deposition of inhaled particles in the lungs. Deposition models agree that particles which are 200 – 300 μm in diameter, have very low deposition in all of the airways, making this nanoparticle aggregate a poor model for lung cells.

Citations

1. Navrotsky, A., *Thermochemistry of nanomaterials.* Nanoparticles and the Environment, 2001. **44**(1): p. 73-103.
2. Singh, S. and H.S. Nalwa, *Nanotechnology and Health Safety – Toxicity and Risk Assessments of Nanostructured Materials on Human Health.* Journal of Nanoscience and Nanotechnology, 2007. **7**(9): p. 3048-3070.
3. Buzea, C., I.I. Pacheco, and K. Robbie, *Nanomaterials and nanoparticles: Sources and toxicity.* Biointerphases, 2007. **2**(4): p. MR17-MR71.
4. Mudunkotuwa, I.A. and V.H. Grassian, *The devil is in the details (or the surface): impact of surface structure and surface energetics on understanding the behavior of nanomaterials in the environment.* Journal of Environmental Monitoring, 2011. **13**(5): p. 1135-44.
5. Keller, A.A., et al., *Global life cycle releases of engineered nanomaterials.* Journal of Nanoparticle Research, 2013. **15**(6).
6. Lee, J., S. Mahendra, and P.J. Alvarez, *Nanomaterials in the construction industry: a review of their applications and environmental health and safety considerations.* ACS Nano, 2010. **4**(7): p. 3580-3590.
7. Sayes, C.M. and D.B. Warheit, *Characterization of nanomaterials for toxicity assessment.* Wiley Interdisciplinary Reviews: Nanomedicine and Nanobiotechnology, 2009. **1**(6): p. 660-70.
8. Huang, X., et al., *The effect of the shape of mesoporous silica nanoparticles on cellular uptake and cell function.* Biomaterials, 2010. **31**(3): p. 438-48.
9. Cho, E.C., et al., *The effects of size, shape, and surface functional group of gold nanostructures on their adsorption and internalization by cells.* Small, 2010. **6**(4): p. 517-22.
10. Ma, Z., et al., *Impact of shape and pore size of mesoporous silica nanoparticles on serum protein adsorption and RBCs hemolysis.* ACS Applied Materials & Interfaces, 2014. **6**(4): p. 2431-8.
11. Hinds, W.C., *Aerosol technology: properties, behavior, and measurement of airborne particles*. 1999: John Wiley & Sons.
12. Maurer-Jones, M.A., et al., *Toxicity of engineered nanoparticles in the environment.* Analytical Chemistry, 2013. **85**(6): p. 3036-49.
13. Murphy, C.J., et al., *Biological Responses to Engineered Nanomaterials: Needs for the Next Decade.* ACS Central Science, 2015. **1**(3): p. 117-123.
14. Garner, K.L. and A.A. Keller, *Emerging patterns for engineered nanomaterials in the environment: a review of fate and toxicity studies.* Journal of Nanoparticle Research, 2014. **16**(8).
15. Nel, A., et al., *Toxic potential of materials at the nanolevel.* Science, 2006. **311**(5761): p. 622-7.
16. Nel, A.E., et al., *Where Are We Heading in Nanotechnology Environmental Health and Safety and Materials Characterization?* ACS Nano, 2015. **9**(6): p. 5627-30.
17. Geary, S.M., A.S. Morris, and A.K. Salem, *Assessing the effect of engineered nanomaterials on the environment and human health.* Journal of Allergy and Clinical Immunology, 2016. **138**(2): p. 405-8.

18. Gunsolus, I.L., et al., *Effects of Humic and Fulvic Acids on Silver Nanoparticle Stability, Dissolution, and Toxicity.* Environmental Science & Technology, 2015. **49**(13): p. 8078-86.
19. Worthington, K.L.S., et al., *Chitosan coating of copper nanoparticles reduces in vitro toxicity and increases inflammation in the lung.* Nanotechnology, 2013. **24**(39): p. 395101.
20. Bian, S.W., et al., *Aggregation and dissolution of 4 nm ZnO nanoparticles in aqueous environments: influence of pH, ionic strength, size, and adsorption of humic acid.* Langmuir, 2011. **27**(10): p. 6059-68.
21. Tso, C.P., et al., *Stability of metal oxide nanoparticles in aqueous solutions.* Water Science and Technology, 2010. **61**(1): p. 127-33.
22. Mudunkotuwa, I.A. and V.H. Grassian, *Citric acid adsorption on TiO2 nanoparticles in aqueous suspensions at acidic and circumneutral pH: surface coverage, surface speciation, and its impact on nanoparticle-nanoparticle interactions.* Journal of the American Chemical Society, 2010. **132**(42): p. 14986-94.
23. Hotze, E.M., T. Phenrat, and G.V. Lowry, *Nanoparticle Aggregation: Challenges to Understanding Transport and Reactivity in the Environment.* Journal of Environment Quality, 2010. **39**(6): p. 1909.
24. Giacomelli, C.E. and W. Norde, *The Adsorption-Desorption Cycle. Reversibility of the BSA-Silica System.* Journal of Colloid and Interface Science, 2001. **233**(2): p. 234-240.
25. Norde, W. and C.E. Giacomelli, *BSA structural changes during homomolecular exchange between the adsorbed and the dissolved states.* Journal of Biotechnology, 2000. **79**(3): p. 259-268.
26. Shi, H., et al., *Titanium dioxide nanoparticles: a review of current toxicological data.* Particle and Fibre Toxicology, 2013. **10**: p. 15.
27. De, M., P.S. Ghosh, and V.M. Rotello, *Applications of Nanoparticles in Biology*. Advanced Materials, 2008. **20**(22): p. 4225-4241.
28. Tan, W., et al., *Bionanotechnology based on silica nanoparticles.* Medical Research Reviews, 2004. **24**(5): p. 621-38.
29. Lin, W., et al., *In vitro toxicity of silica nanoparticles in human lung cancer cells.* Toxicology and Applied Pharmacology, 2006. **217**(3): p. 252-9.
30. Patwardhan, S.V., et al., *Chemistry of aqeuous silica nanoparticle surfaces and the mechanism of selective peptide adsorption.* Journal of the American Chemical Society, 2012. **134**: p. 6244-56.
31. Karimi, M., et al., *Albumin nanostructures as advanced drug delivery systems.* Expert Opinion on Drug Delivery, 2016: p. 1-15.
32. Mahon, E., et al., *Designing the nanoparticle-biomolecule interface for "targeting and therapeutic delivery"*. Journal of Controlled Release, 2012. **161**(2): p. 164-74.
33. Islam, N. and V. Ferro, *Recent advances in chitosan-based nanoparticulate pulmonary drug delivery.* Nanoscale, 2016. **8**(30): p. 14341-58.
34. Klassen, C. and J.B.I. Watkins, *Casarett & Doull's Essentials of Toxicology*. 3 ed. 2015: McGraw-Hill Education / Medical. 528.
35. Giard, D.J., et al., *In vitro cultivation of human tumors: establishment of cell lines derived from a series of solid tumors.* Journal of the National Cancer Institute, 1973. **51**(5): p. 1417-23.
36. Caban, S., et al., *Nanosystems for Drug Delivery.* OA Drug Design and Delivery, 2014. **2**(1).

37. Gehr, P., et al., *Particle-Lung Interactions, Second Edition*. 2009: Informa Healthcare, New York, NY.
38. Tsuda, A. and P. Gehr, *Nanoparticles in the Lung*. 2015: CRC Press, Taylor & Francis, Boca Raton, FL.
39. Muhlfeld, C., P. Gehr, and B. Rothen-Rutishauser, *Translocation and cellular entering mechanisms of nanoparticles in the respiratory tract.* Swiss Medical Weekly, 2008. **138**(27-28): p. 387-91.
40. Sakamoto, A., et al., *Drug Transporter Protein Quantification of Immortalized Human Lung Cell Lines Derived from Tracheobronchial Epithelial Cells (Calu-3 and BEAS2-B), Bronchiolar-Alveolar Cells (NCI-H292 and NCI-H441), and Alveolar Type II-like Cells (A549) by Liquid Chromatography-Tandem Mass Spectrometry*. Journal of Pharmaceutical Sciences, 2015.
41. Hillaireau, H. and P. Couvreur, *Nanocarriers' entry into the cell: relevance to drug delivery*. Cellular and Molecular Life Sciences, 2009. **66**(17): p. 2873-96.
42. Shang, L., et al., *Nanoparticles Interacting with Proteins and Cells: A Systematic Study of Protein Surface Charge Effects.* Advanced Materials Interfaces, 2014. **1**(2): p. n/a-n/a.
43. Lynch, I. and K.A. Dawson, *Protein-nanoparticle interactions.* Nano Today, 2008. **3**(1-2): p. 40-47.
44. Lundqvist, M., et al., *Nanoparticle size and surface properties determine the protein corona with possible implications for biological impacts.* Proceedings of the National Academy of Sciences, 2008. **105**(38): p. 14265-70.
45. Hellstrand, E., et al., *Complete high-density lipoproteins in nanoparticle corona.* FEBS Journal, 2009. **276**(12): p. 3372-81.
46. Monopoli, M.P., et al., *Biomolecular coronas provide the biological identity of nanosized materials.* Nature Nanotechnology, 2012. **7**(12): p. 779-86.
47. Walczyk, D., et al., *What the Cell "Sees" in Bionanoscience.* Journal of the American Chemical Society, 2010. **132**(16): p. 5761-5768.
48. Walkey, C.D., et al., *Protein corona fingerprinting predicts the cellular interaction of gold and silver nanoparticles.* ACS Nano, 2014. **8**(3): p. 2439-55.
49. Walkey, C.D. and W.C. Chan, *Understanding and controlling the interaction of nanomaterials with proteins in a physiological environment.* Chemical Society Reviews, 2012. **41**(7): p. 2780-99.
50. Lee, Y.K., et al., *Effect of the protein corona on nanoparticles for modulating cytotoxicity and immunotoxicity.* International Journal of Nanomedicine, 2015. **10**: p. 97-113.
51. Lehman, S.E., et al., *Nano-Bio Interactions of Porous and Nonporous Silica Nanoparticles of Varied Surface Chemistry: A Structural, Kinetic, and Thermodynamic Study of Protein Adsorption from RPMI Culture Medium.* Langmuir, 2016. **32**(3): p. 731-42.
52. Lundqvist, M., et al., *The evolution of the protein corona around nanoparticles: a test study.* ACS Nano, 2011. **5**(9): p. 7503-9.
53. Tenzer, S., et al., *Nanoparticle Size Is a Critical Physicochemical Determinant of the Human Blood Plasma Corona: A Comprehensive Quantitative Proteomic Analysis.* ACS Nano, 2011. **5**(9): p. 7155-7167.
54. Lesniak, A., et al., *Serum heat inactivation affects protein corona composition and nanoparticle uptake.* Biomaterials, 2010. **31**(36): p. 9511-8.

55. Maiorano, G., et al., *Effects of cell culture media on the dynamic formation of protein-nanoparticle complexes and influence on the cellular response.* ACS Nano, 2010. **4**(12): p. 7481-91.
56. Slowing, I., B.G. Trewyn, and V.S. Lin, *Effect of surface functionalization of MCM-41-type mesoporous silica nanoparticles on the endocytosis by human cancer cells.* Journal of the American Chemical Society, 2006. **128**(46): p. 14792-3.
57. Silva, J.M., et al., *Immune system targeting by biodegradable nanoparticles for cancer vaccines.* Journal of Controlled Release, 2013. **168**(2): p. 179-99.
58. Dominguez-Medina, S., et al., *Adsorption of a Protein Monolayer via Hydrophobic Interactions Prevents Nanoparticle Aggregation under Harsh Environmental Conditions.* ACS Sustainable Chemistry & Engineering, 2013. **1**(7): p. 833-842.
59. Harrington, W., P. Johnson, and R. Ottewill, *Bovine serum albumin and its behaviour in acid solution.* Biochemical Journal, 1956. **62**(4): p. 569.
60. Slayter, E.M., *An electron microscope study of the conformational change in bovine serum albumin at low pH.* Journal of Molecular Biology, 1965. **14**: p. 443-452.
61. Mudunkotuwa, I.A., A. Al Minshid, and V.H. Grassian, *ATR-FTIR spectroscopy as a tool to probe surface adsorption on nanoparticles at the liquid-solid interface in environmentally and biologically relevant media.* Analyst, 2014. **139**(5): p. 870-881.
62. Mudunkotuwa, I.A. and V.H. Grassian, *Histidine adsorption on TiO2 nanoparticles: an integrated spectroscopic, thermodynamic, and molecular-based approach toward understanding nano-bio interactions.* Langmuir, 2014. **30**(29): p. 8751-60.
63. Baker, M.J., et al., *Using Fourier transform IR spectroscopy to analyze biological materials.* Nature Protocols, 2014. **9**(8): p. 1771-91.
64. Yang, H., et al., *Obtaining information about protein secondary structures in aqueous solution using Fourier transform IR spectroscopy.* Nature Protocols, 2015. **10**(3): p. 382-96.
65. Glassford, S.E., B. Byrne, and S.G. Kazarian, *Recent applications of ATR FTIR spectroscopy and imaging to proteins.* Biochimica et Biophysica Acta, 2013. **1834**(12): p. 2849-58.
66. Napierska, D., et al., *The nanosilica hazard: another variable entity.* Particle and Fibre Toxicology, 2010. **7**(1): p. 39.
67. Roach, P., D. Farrar, and C.C. Perry, *Interpretation of protein adsorption: surface-induced conformational changes.* Journal of the American Chemical Society, 2005. **127**(22): p. 8168-73.
68. Roach, P., D. Farrar, and C.C. Perry, *Surface tailoring for controlled protein adsorption: Effect of topography at the nanometer scale and chemistry.* Journal of the American Chemical Society, 2006. **128**(12): p. 3939-3945.
69. Norde, W., *My voyage of discovery to proteins in flatland ...and beyond.* Colloids and Surfaces B: Biointerfaces, 2008. **61**(1): p. 1-9.
70. Braydich-Stolle, L.K., et al., *Dynamic characteristics of silver nanoparticles in physiological fluids: toxicological implications.* Langmuir, 2014. **30**(50): p. 15309-16.
71. Schaeublin, N.M., et al., *Surface charge of gold nanoparticles mediates mechanism of toxicity.* Nanoscale, 2011. **3**(2): p. 410-20.
72. Park, H.J., et al., *Acute exposure to silica nanoparticles aggravate airway inflammation: different effects according to surface characteristics.* Experimental & Molecular Medicine, 2015. **47**: p. e173.

73. Mudunkotuwa, I.A. and V.H. Grassian, *Biological and environmental media control oxide nanoparticle surface composition: the roles of biological components (proteins and amino acids), inorganic oxyanions and humic acid.* Environmental Science: Nano, 2015. **2**(5): p. 429-439.
74. Bremer, M.G.E.G., et al., *Electrostatic interactions between immunoglobulin (IgG) molecules and a charged sorbent.* Colloids and Surfaces A: Physicochemical and Engineering Aspects, 2004. **250**(1-3): p. 29-42.
75. Rimola, A., M. Sodupe, and P. Ugliengo, *Affinity Scale for the Interaction of Amino Acids with Silica Surfaces.* Journal of Physical Chemistry C, 2009. **113**(14): p. 5741-5750.
76. Mueller, R., et al., *OH surface density of SiO2 and TiO2 by thermogravimetric analysis.* Langmuir, 2003. **19**(1): p. 160-165.
77. Jackson, M. and H.H. Mantsch, *The Use and Misuse of Ftir Spectroscopy in the Determination of Protein-Structure.* Critical Reviews in Biochemistry and Molecular Biology, 1995. **30**(2): p. 95-120.
78. Lundqvist, M., I. Sethson, and B.H. Jonsson, *Protein adsorption onto silica nanoparticles: conformational changes depend on the particles' curvature and the protein stability.* Langmuir, 2004. **20**(24): p. 1063-10647.
79. Petushkov, A., et al., *Effect of crystal size and surface functionalization on the cytotoxicity of silicalite-1 nanoparticles.* Chemical Research in Toxicology, 2009. **22**(7): p. 1359-68.
80. Su, T.J., et al., *Effect of pH on the adsorption of bovine serum albumin at the silica/water interface studied by neutron relfection.* Journal of Physical Chemistry B, 1990. **103**: p. 3727-3736.
81. Wiśniewska, M., K. Szewczuk-Karpisz, and D. Sternik, *Adsorption and thermal properties of the bovine serum albumin–silicon dioxide system.* Journal of Thermal Analysis and Calorimetry, 2014. **120**(2): p. 1355-1364.
82. Fukuzaki, S., H. Urano, and K. Nagata, *Adsorption of bovine serum albumin onto metal oxide surfaces.* Journal of Fermentation and Bioengineering, 1996. **81**(2): p. 163-167.
83. Moulton, S.E., et al., *ATR-IR spectroscopic studies of the influence of phosphate buffer on adsorption of immunoglobulin G to TiO2.* Colloids and Surfaces A: Physicochemical and Engineering Aspects, 2003. **220**(1-3): p. 159-167.
84. Kong, J. and S. Yu, *Fourier transform infrared spectroscopic analysis of protein secondary stuctures.* Acta Biochimica et Biophysica Sinica, 2007. **39**(8): p. 549-559.
85. Kitadai, N., T. Yokoyama, and S. Nakashima, *ATR-IR spectroscopic study of L-lysine adsorption on amorphous silica.* Journal of Colloid and Interface Science, 2009. **329**(1): p. 31-7.
86. Guo, C. and G.P. Holland, *Investigating Lysine Adsorption on Fumed Silica Nanoparticles.* Journal of Physical Chemistry C, 2014. **118**(44): p. 25792-25801.
87. Brown, J.R., *Serum Albumin: Amino Acid Sequence*, in *Albumin: Structure, Function and Uses*, V.M. Rosenoer, M. Oratz, and M.A. Rothschild, Editors. 1977, Pergamon Press. p. 27-51.
88. Dekali, S., et al., *Cell cooperation and role of the P2X(7) receptor in pulmonary inflammation induced by nanoparticles.* Nanotoxicology, 2013. **7**(8): p. 1302-14.
89. Guadagnini, R., et al., *Toxicity evaluation of engineered nanoparticles for medical applications using pulmonary epithelial cells.* Nanotoxicology, 2015. **9**: p. 25-32.

90. Bancos, S., D.L. Stevens, and K.M. Tyner, *Effect of silica and gold nanoparticles on macrophage proliferation, activation markers, cytokine production, and phagocytosis in vitro.* International Journal of Nanomedicine, 2015. **10**: p. 183-206.
91. Tirtaatmadja, N., et al., *Nanoparticles-induced inflammatory cytokines in human plasma concentration manner: an ignored factor at the nanobio-interface.* Journal of the Iranian Chemical Society, 2014. **12**(2): p. 317-323.
92. Kasper, J., et al., *Interactions of silica nanoparticles with lung epithelial cells and the association to flotillins.* Archives of Toxicology, 2013. **87**(6): p. 1053-65.
93. Shang, L., K. Nienhaus, and G.U. Nienhaus, *Engineered nanoparticles interacting with cells: size matters.* Journal of Nanobiotechnology, 2014. **12**(5): p. 5.
94. Arnida, A.M. and H. Ghandehari, *Cellular uptake and toxicity of gold nanoparticles in prostate cancer cells: a comparative study of rods and spheres.* Journal of Applied Toxicology, 2010. **30**(3): p. 212-7.
95. Singh, S., et al., *Endocytosis, oxidative stress and IL-8 expression in human lung epithelial cells upon treatment with fine and ultrafine TiO2: role of the specific surface area and of surface methylation of the particles.* Toxicology and Applied Pharmacology, 2007. **222**(2): p. 141-51.
96. Horie, M., et al., *Protein Adsorption of Ultrafine Metal Oxide and Its Influence on Cytotoxicity toward Cultured Cells.* Chemical Research in Toxicology, 2009. **22**(3): p. 543-553.
97. Akhtar, M.J., et al., *Nanotoxicity of pure silica mediated through oxidant generation rather than glutathione depletion in human lung epithelial cells.* Toxicology, 2010. **276**(2): p. 95-102.
98. Gonzalez, L., et al., *Exploring the aneugenic and clastogenic potential in the nanosize range: A549 human lung carcinoma cells and amorphous monodisperse silica nanoparticles as models.* Nanotoxicology, 2010. **4**: p. 382-95.
99. Lesniak, A., et al., *Effects of the presence or absence of a protein corona on silica nanoparticle uptake and impact on cells.* ACS Nano, 2012. **6**(7): p. 5845-57.
100. Uboldi, C., et al., *Amorphous silica nanoparticles do not induce cytotoxicity, cell transformation or genotoxicity in Balb/3T3 mouse fibroblasts.* Mutation Research, 2012. **745**(1-2): p. 11-20.
101. Schmaljohann, D., *Thermo- and pH-responsive polymers in drug delivery.* Advanced Drug Delivery Reviews, 2006. **58**(15): p. 1655-70.
102. Stebounova, L.V., E. Guio, and V.H. Grassian, *Silver nanoparticles in simulated biological media: a study of aggregation, sedimentation, and dissolution.* Journal of Nanoparticle Research, 2010. **13**(1): p. 233-244.
103. Podila, R., et al., *Illuminating nano-bio interactions: A spectroscopic perspective.* MRS Bulletin, 2014. **39**(11): p. 990-995.
104. Saptarshi, S.R., A. Duschl, and A.L. Lopata, *Interaction of nanoparticles with proteins: relation to bio-reactivity of the nanoparticle.* Journal of Nanobiotechnology, 2013. **11**(26): p. 26.
105. Jachimska, B. and A. Pajor, *Physico-chemical characterization of bovine serum albumin in solution and as deposited on surfaces.* Bioelectrochemistry, 2012. **87**: p. 138-46.
106. Carter, D.C. and J.X. Ho, *Structure of serum albumin.* Advances in Protein Chemistry, 1994. **45**: p. 153-203.

107. Abramoff, M.D., P.J. Magalhaes, and S.J. Ram, *Image Processing with ImageJ*. Biophotonics International, 2004. 11(7): p. 36-42.
108. Salgin, S., U. Salgin, and S. Bahadir, *Zeta Potentials and Isoelectric Points of Biomolecules: The Effects of Ion Types and Ionic Strengths.* International Journal of Electrochemical Science, 2012. **7**(12): p. 12404-12414.
109. Kosmulski, M., *The pH-dependent surface charging and the points of zero charge.* Journal of Colloid and Interface Science, 2002. **253**(1): p. 77-87.
110. Ge, S., et al., *Bovine serum albumin adsorption onto immobilized organotrichlorosilane surface: influence of the phase separation on protein adsorption patterns.* Journal of Biomaterials Science, Polymer Edition, 1998. **9**(2): p. 131-150.
111. Goodman, C.M., et al., *Toxicity of gold nanoparticles functionalized with cationic and anionic side chains.* Bioconjugate Chemistry, 2004. **15**(4): p. 897-900.
112. Steiner, G., et al., *Conformational changes during protein adsorption FTIR spectroscopic imaging of adsorbed fibrinogen layers.* Analytical Chemistry, 2007: p. 1311-1316.
113. Bouhekka, A. and T. Bürgi, *In situ ATR-IR spectroscopy study of adsorbed protein: Visible light denaturation of bovine serum albumin on TiO2.* Applied Surface Science, 2012. **261**: p. 369-374.
114. Demanèche, S., et al., *Dissimilar pH-dependent adsorption features of bovine serum albumin and α-chymotrypsin on mica probed by AFM.* Colloids and Surfaces B: Biointerfaces, 2009. **70**(2): p. 226-231.
115. Zhang, H., et al., *Use of metal oxide nanoparticle band gap to develop a predictive paradigm for oxidative stress and acute pulmonary inflammation.* ACS Nano, 2012. **6**(5): p. 4349-4368.
116. Long, T.C., et al., *Titanium dioxide (P25) produces reactive oxygen species in immortalized brain microglia (BV2): implications for nanoparticle neurotoxicity.* Environmental Science & Technology, 2006. **40**(14): p. 4346-4352.
117. Macwan, D., P.N. Dave, and S. Chaturvedi, *A review on nano-TiO2 sol–gel type syntheses and its applications.* Journal of Materials Science, 2011. **46**(11): p. 3669-3686.
118. Lomer, M.C.E., R.P.H. Thompson, and J.J. Powell, *Fine and ultrafine particles of the diet: influence on the mucosal immune response and association with Crohn's disease.* Proceedings of the Nutrition Society, 2002. **61**(1): p. 123-130.
119. Oberdörster, G., E. Oberdörster, and J. Oberdörster, *Nanotoxicology: an emerging discipline evolving from studies of ultrafine particles.* Environmental Health Perspectives, 2005: p. 823-839.
120. Warheit, D.B., et al., *Health effects related to nanoparticle exposures: environmental, health and safety considerations for assessing hazards and risks.* Pharmacology & Therapeutics, 2008. **120**(1): p. 35-42.
121. Fu, F.-N., et al., *Secondary Structure Estimation of Proteins Using the Amide III Region of Fourier Transform Infrared Spectroscopy: Application to Analyze Calcium-Binding-Induced Structural Changes in Calsequestrin.* Applied Spectroscopy, 1994. **48**(11): p. 1432-1441.
122. Schwinte, P., et al., *Stabilizing effects of various polyelectrolyte multilayer films on the structure of adsorbed/embedded fibrinogen molecules: an ATR-FTIR study.* Journal of Physical Chemistry B, 2001. **105**(47): p. 11906-11916.
123. Barth, A., *Infrared spectroscopy of proteins.* Biochimica et Biophysica Acta, 2007. **1767**(9): p. 1073-101.

124. Qing, H., et al., *Effects of pH and metal ions on the conformation of bovine serum albumin in aqueous solution An attenuated total reflection (ATR) FTIR spectroscopic study.* Spectrochimica Acta Part A: Molecular and Biomolecular Spectroscopy, 1996. **52**(13): p. 1795-1800.
125. Zeng, H., K.K. Chittur, and W.R. Lacefield, *Analysis of bovine serum albumin adsorption on calcium phosphate and titanium surfaces.* Biomaterials, 1999. **20**(4): p. 377-84.
126. Kang, Y., et al., *On the Mechanism of Protein Adsorption onto Hydroxylated and Nonhydroxylated TiO2 Surfaces.* Journal of Physical Chemistry C, 2010. **114**(34): p. 14496-14502.
127. Xu, Y., et al., *The role of protein characteristics in the formation and fluorescence of Au nanoclusters.* Nanoscale, 2014. **6**(3): p. 1515-1524.
128. Wright, A.K. and M.R. Thompson, *Hydrodynamic stucture of bovine serum albumin determined by tansiet electric birfringence.* Biophysical Journal, 1975. **15**.
129. Gulseren, I., et al., *Structural and functional changes in ultrasonicated bovine serum albumin solutions.* Ultrasonics Sonochemistry, 2007. **14**(2): p. 173-83.
130. Murayama, K., et al., *Two-dimensional/attenuated total reflection infrared correlation spectroscopy studies on secondary structural changes in human serum albumin in aqueous solutions: pH-dependent structural changes in the secondary structures and in the hydrogen bondings of side chains.* Journal of Physical Chemistry B, 2001. **105**(20): p. 4763-4769.
131. Peters, T., Jr., *All About Albumin: Biochemistry, Genetics, and Medical Applications*. 1995: Academic Press, San Diego, CA.
132. Takeda, K., et al., *Conformational change of bovine serum albumin by heat treatment.* Journal of Protein Chemistry, 1989. **8**(5): p. 653-9.
133. Nakamura, K., et al., *Conformational changes in seventeen cystine disulfide bridges of bovine serum albumin proved by Raman spectroscopy.* FEBS Letters, 1997. **417**(3): p. 375-378.
134. Sogami, M. and J.F. Foster, *Isomerization Reactions of Charcoal-Defatted Bovine Plasma Albumin. The N-F Trnasition and Acid Expansion.* Biochemistry, 1968. **7**(6).
135. Hong, Y., et al., *Surface hydroxyl groups direct cellular response on amorphous and anatase TiO2 nanodots.* Colloids and Surfaces B: Biointerfaces, 2014. **123**: p. 68-74.
136. Kubiak-Ossowska, K. and P.A. Mulheran, *What governs protein adsorption and immobilization at a charged solid surface?* Langmuir, 2010. **26**(11): p. 7690-4.
137. Fleischer, C.C. and C.K. Payne, *Nanoparticle-cell interactions: molecular structure of the protein corona and cellular outcomes.* Accounts of Chemical Research, 2014. **47**(8): p. 2651-9.
138. Sebben, D. and P. Pendleton, *Analysis of ionic strength effects on the adsorption of simple amino acids.* Journal of Colloid and Interface Science, 2015. **443**: p. 153-61.
139. El Kadi, N., et al., *Unfolding and refolding of bovine serum albumin at acid pH: ultrasound and structural studies.* Biophysical Journal, 2006. **91**(9): p. 3397-404.
140. Chittur, K.K., *FTIR/ATR for protein adsorption to biomaterial surfaces.* Biomaterials, 1998. **19**(4-5): p. 357-69.
141. Kurrat, R., J.E. Prenosil, and J.J. Ramsden, *Kinetics of Human and Bovine Serum Albumin Adsorption at Silica–Titania Surfaces.* Journal of Colloid and Interface Science, 1997. **185**(1): p. 1-8.

142. Wassell, D.T. and G. Embery, *Adsorption of bovine serum albumin on to titanium powder.* Biomaterials, 1996. **17**(9): p. 859-64.
143. Stone, V., H. Johnston, and M.J. Clift, *Air pollution, ultrafine and nanoparticle toxicology: cellular and molecular interactions.* IEEE Transactions on NanoBioscience, 2007. **6**(4): p. 331-340.
144. Vallee, A., V. Humblot, and C.M. Pradier, *Peptide interactions with metal and oxide surfaces.* Accounts of Chemical Research, 2010. **43**(10): p. 1297-306.
145. Xu, M., et al., *Formation of nano-bio-complex as nanomaterials dispersed in a biological solution for understanding nanobiological interactions.* Scientific Reports, 2012. **2**: p. 406.
146. Metin, C.O., et al., *Stability of aqueous silica nanoparticle dispersions.* Journal of Nanoparticle Research, 2010. **13**(2): p. 839-850.
147. Connor, P.A., K.D. Dobson, and A.J. McQuillan, *Infrared spectroscopy of the TiO2/aqueous solution interface.* Langmuir, 1999. **15**(7): p. 2402-2408.
148. Bergstrom, L., *Hamaker constants of inorganic materials.* Advances in Colloid and Interface Science, 1997. **70**: p. 125-169.
149. Mudunkotuwa, I.A., ***Engineered metal based nanomateirals in aqueous environments: interactions, transformations, and implications***, in *Chemistry*. 2013, University of Iowa. p. 156.
150. Phenrat, T., et al., *Stabilization of aqueous nanoscale zerovalent iron dispersions by anionic polyelectrolytes: adsorbed anionic polyelectrolyte layer properties and their effect on aggregation and sedimentation.* Journal of Nanoparticle Research, 2007. **10**(5): p. 795-814.
151. Morez, S.T., et al., *Formation Mechanism for Stable Hybrid Clusters of Proteins and Nanoparticles.* ACS Nano, 2015. **9**(7): p. 6696-6705.
152. Tester, J.W. and M. Modell, *Thermodynamics and Its Applications*. 3 ed. Prentice Hall International Series inthe Physical and Chemical Engineering Sciences, ed. N.R. Amundson. Upper Saddle River, New Jersey: Prentice Hall PTR. 935.
153. Shah, P.S., et al., *Size-selective dispersion of dodecanethiol-coated nanocrystals in liquid and supercritical ethane by density tuning.* Journal of Physical Chemistry B, 2002. **106**(10): p. 2545-2551.
154. Cohen, J.M., J.G. Teeguarden, and P. Demokritou, *An integrated approach for the in vitro dosimetry of engineered nanomaterials.* Particle and Fibre Toxicology, 2014. **11**: p. 20.
155. Lewinski, N., V. Colvin, and R. Drezek, *Cytotoxicity of nanoparticles.* Small, 2008. **4**(1): p. 26-49.
156. Freese, C., et al., *In vitro investigation of silica nanoparticle uptake into human endothelial cells under physiological cyclic stretch.* Particle and Fibre Toxicology, 2014. **11**: p. 68.
157. Auffan, M., et al., *Chemical stability of metallic nanoparticles: a parameter controlling their potential cellular toxicity in vitro.* Environmental Pollution, 2009. **157**(4): p. 1127-33.
158. Warheit, D.B., *Inhaled Amorphous Silica Particulates:What Do We Know About Their Toxicological Profiles?* 2001. **20**(Suppl.1): p. 9.
159. Brandenberger, C., et al., *Engineered silica nanoparticles act as adjuvants to enhance allergic airway disease in mice.* Particle and Fibre Toxicology, 2013. **10**(26): p. 26.
160. Chang, J., et al., *In vitro cytotoxicity of silica nanoparticles at high concentrations strongly depend on the metabolic activity type of the cell line.* Environmental Science & Technology, 2007. **41**(6): p. 2064-8.

161. Drescher, D., et al., *Toxicity of amorphous silica nanoparticles on eukaryotic cell model is determined by particle agglomeration and serum protein adsorption effects.* Analytical and Bioanalytical Chemistry, 2011. **400**(5): p. 1367-73.
162. Jin, Y., et al., *Toxicity of luminescent silica nanoparticles to living cells.* Chemical Research in Toxicology, 2007. **20**(8): p. 1126-33.
163. Li, Y., et al., *Size-dependent cytotoxicity of amorphous silica nanoparticles in human hepatoma HepG2 cells.* Toxicology In Vitro, 2011. **25**(7): p. 1343-52.
164. Paula, A.J., et al., *Influence of protein corona on the transport of molecules into cells by mesoporous silica nanoparticles.* ACS Applied Materials & Interfaces, 2013. **5**(17): p. 8387-93.
165. Shi, Y., et al., *Endotoxin promotes adverse effects of amorphous silica nanoparticles on lung epithelial cells in vitro.* Journal of Toxicology and Environmental Health, Part A, 2010. **73**(11): p. 748-56.
166. Shi, J., et al., *Hemolytic properties of synthetic nano- and porous silica particles: the effect of surface properties and the protection by the plasma corona.* Acta Biomaterialia, 2012. **8**(9): p. 3478-90.
167. Geiser, M. and W.G. Kreyling, *Deposition and biokinetics of inhaled nanoparticles.* Particle and Fibre Toxicology, 2010. **7**: p. 2.
168. Kreyling, W.G. and M. Geiser, *Dosimetry of Inhaled Nanoparticles*, in *Nanoparticles in medicine and environment: Inhalantion and health effects*, J.C. Marijnissen and L. Gradon, Editors. 2009, Springer.
169. Love, S.A., et al., *Assessing nanoparticle toxicity.* Annual Review of Analytical Chemistry (Palo Alto Calif), 2012. **5**: p. 181-205.
170. Wang, S., H. Yu, and J.K. Wickliffe, *Limitation of the MTT and XTT assays for measuring cell viability due to superoxide formation induced by nano-scale TiO2.* Toxicology In Vitro, 2011. **25**(8): p. 2147-51.
171. Worle-Knirsch, J.M., K. Pulskamp, and H.F. Krug, *Oops they did it again! Carbon nanotubes hoax scientists in viability assays.* Nano Letters, 2006. **6**(6): p. 1261-1268.
172. Wongrakpanich, A., et al., *Size-dependent cytotoxicity of copper oxide nanoparticles in lung epithelial cells.* Environmental Science: Nano, 2016.